

IN SITU CRYSTALLIZATION OF NATIVE POLY(3-HYDROXYBUTYRATE) GRANULES
IN VARYING ENVIRONMENTAL CONDITIONS

A THESIS SUBMITTED TO THE GRADUATE DIVISION OF THE
UNIVERSITY OF HAWAI'I AT MĀNOA IN PARTIAL FULFILLMENT
OF THE REQUIREMENTS FOR THE DEGREE OF

MASTER OF SCIENCE

IN

BIOLOGICAL ENGINEERING

DECEMBER 2010

By

Michael M Porter

Thesis Committee:

Jian Yu, Chairperson

Stephen Masutani

Samir Khanal

ACKNOWLEDGEMENTS

I would like to thank Jian Yu from Hawai'i Natural Energy Institute (HNEI) for providing much appreciated work space and guidance throughout the course of this research. I would also like to thank my committee members, Stephen Masutani and Samir Khanal, for their suggestions and support; Matt Jaremko from HNEI for providing the PHB-containing cells; Qiang Liu from Agriculture and Agri-Food, Canada for the DSC analysis; and Tina Carvalho from the Biological Electron Microscope Facility (BEMF) for her assistance with the TEM/SEM images. This research was partially supported by the Consortium for Plant Biotechnology Research (CPBR) and the U.S. Department of Energy.

ABSTRACT

Poly(3-hydroxybutyrate) (PHB) is a microbial biopolyester that can be produced from renewable feedstocks as an eco-friendly bioplastic. PHB *in vivo* exists as amorphous, intracellular granules that contain a small amount of water and are surrounded by a membrane of lipids and proteins. The native granules undergo varying degrees of crystallization when subjected to changes in environment such as dehydration, temperature, pH, and other mild conditions. For the first time, the *in situ* crystallization of native PHB granules was monitored via ATR-FTIR. Empirical models describing the crystallization of PHB granules in different environments were developed from Avrami's equation. The extent of granule crystallization is governed by granule size, number of nucleation points, and spherulitic geometry. The primary stabilizing factors of amorphous PHB granules are water, membrane lipids and proteins. Removing any of these factors may induce partial crystallization of PHB, which toughens the granules against extensive molecule degradation and granule aggregation.

TABLE OF CONTENTS

ACKNOWLEDGEMENTS	ii
ABSTRACT	iii
LIST OF TABLES	vi
LIST OF FIGURES	vii-ix
LIST OF ABBREVIATIONS AND SYMBOLS	x-xi
CHAPTER 1 INTRODUCTION	1-10
1.1 Bioplastics and Polyhydroxyalkanoates (PHA)	1-2
1.2 Poly(3-hydroxybutyrate) (PHB)	2-5
1.3 PHB Granules	5-6
1.4 Monitoring PHB Crystallization with ATR-FTIR	6-7
1.5 Modeling PHB Crystallization.....	7-9
1.6 Research Objective	9-10
CHAPTER 2 MATERIALS AND METHODS	11-14
2.1 PHB Granules	11
2.2 Purified PHA	11-12
2.3 Chemical Analysis.....	12
2.4 ATR-FTIR Spectroscopy	12-13
2.5 Differential Scanning Calorimetry (DSC)	13
2.6 Viscosity-average Molecular Weight	13
2.7 Transmission Electron Microscopy (TEM)	13-14
2.8 Scanning Electron Microscopy (SEM)	14
CHAPTER 3 MONITORING PHB CRYSTALLIZATION WITH ATR-FTIR	15-23
3.1 Fourier Transform Infrared Spectroscopy (FTIR) and Attenuated Total Reflectance (ATR)	15-17
3.2 Molecular Vibrational Energy	17-18
3.3 Monitoring the Crystallization of Pure PHB with ATR-FTIR	19-21
3.4 ATR-FTIR/DSC Crystallinity Correlation	21-23

3.5	Monitoring the <i>In Situ</i> Crystallization of Native PHB Granules with ATR-FTIR	23-26
3.6	<i>In Situ</i> Crystallinity Measurements via ATR-FTIR Absorption Spectra	26-27
CHAPTER 4	CRYSTALLIZATION OF PHB	28-45
4.1	Crystallization of Pure PHB	28-30
4.2	<i>In Situ</i> Crystallization of Native PHB Granules	30-32
4.3	Modeling the <i>In Situ</i> Crystallization of PHB Granules in Different Environments	33-40
	4.3.1 <i>Heated PHB Granules</i>	33-37
	4.3.2 <i>Alkaline PHB Granules</i>	37-40
4.4	Interpretation of Avrami Exponents and Growth Rate Parameters	40-45
CHAPTER 5	BEHAVIOR OF PHB GRANULES IN MILD CONDITIONS	46-48
5.1	Centrifuged PHB Granules	46-47
5.2	Ultrasonicated PHB Granules	47
5.3	PHB Granules with Surfactant	48
CHAPTER 6	PROPERTIES OF PHB GRANULES OF DIFFERENT CRYSTALLINITY	49-52
6.1	Granules Morphology	49-51
6.2	Molecule Degradation	51-52
CHAPTER 7	PRACTICAL APPLICATIONS OF THE <i>IN SITU</i> CRYSTALLIZATION OF PHB	53-55
CHAPTER 8	FUTURE WORK	56
REFERENCES	57-58

LIST OF TABLES

1	Typical material properties of PHBV with varying fractions of 3HV [2].....	3
2	Infrared absorption indices, thermal properties, and crystallinity of pure PHA samples	22
3	ATR-FTIR/DSC crystallinity correlation values	23
4	Slurry properties of native PHB granules from different aqueous media (0.2 M H ₂ SO ₄)	31
5	Crystallization parameters of the heated PHB granules (slurry A) from Avrami analysis.....	37
6	Crystallization parameters of the PHB granules (slurry B) with increasing pH from Avrami analysis	40
7	Crystallization models of pure PHB and PHB granules in varying environments by Avrami analysis	41
8	Crystallinity and state of granule membrane versus granule morphology (i.e., aggregation) ..	49
9	Addition of surfactant (SDS) during PHB recovery treatments.....	54

LIST OF FIGURES

1	TEM images of microbial cells containing PHA granules	2
2	General chemical structure of polyhydroxyalkanoates, the monomers 3HB and 3HV, and a copolymer 3HB-co-3HV [8]	2
3	Amorphous and crystalline regions of a semi-crystalline polymer such as PHB [10, 11, 15-17] ..	4
4	(a) TEM image of native PHB granules in microbial cells, illustrating the bilayer membrane surrounding each cell and the monolayer membrane surrounding each granule; (b) schematic of a native PHB granule, illustrating the intra-granule water, membrane lipids and proteins [3, 6, 21-23]	5
5	Some common vibrational modes associated with PHB: (a) C=O stretching; (b) C–O–C asymmetric stretching; (c) C–O–C symmetric stretching; (d) CH ₃ symmetric bending; (e) CH ₃ asymmetric bending [30, 31]	7
6	Schematic of a spherulite, illustrating the nucleus, lamellae, and direction of growth [11, 20]	8
7	Crystallization of PHBV from melt at 100°C after (a) 3 min, (b) 7 min, (c) 15 min, and (d) 3 hr	8
8	Schematic of attenuated total reflectance with single internal reflection [31]	17
9	Simple harmonic oscillator: (a) compression ($x < 0$); (b) equilibrium ($x = 0$); (c) extension ($x > 0$)	18
10	Time development of the infrared absorption spectra of pure PHB illustrating the crystallization due to cooling from an amorphous melt at 180°C (solid line) to a semi-crystalline solid at room temperature (dashed line) in ambient conditions	19
11	ATR-FTIR absorption index versus DSC crystallinity from pure PHA samples.....	22
12	TEM images of PHB-containing cells: (a) in neutral solution (pH 7); (b) in acidic solution (pH 2)	23
13	Time development of the infrared absorption spectra of PHB-containing cells suspended in acidic solution illustrating the initial spectrum dominated by water at 0 mins (dotted line), the secondary spectrum characteristic of the instantaneous crystallinity after 10 mins (solid line), and the final spectrum caused by extensive dehydration after 30 mins (dashed line)	24
14	Infrared absorption and water fraction of PHB-containing cells suspended in acidic solution versus measurement time, illustrating three spectral regions: initial (stage 1), where PHB-containing cells are suspended in aqueous solution and free-water begins to evaporate (0-5 min); secondary (stage 2), where free-water continues to evaporate and PHB-containing cells deposit onto ATR window via sedimentation (5-15 min); and final (stage 3), where excess intra-granule water evaporates causing the PHB granules to crystallize (15-30 min)	25
15	Crystallinity versus time for pure PHB cooled from a melt at 180°C to room temperature in ambient conditions, where ● indicates the primary crystallization region modeled by Avrami's equation.....	29

16	Determination of the crystallization rate constant k and the Avrami exponent n for the crystallization of pure PHB at room temperature during primary crystallization	30
17	<i>In situ</i> crystallinity versus measurement time for native PHB granules in acidic solution (pH 2) at room temperature, illustrating the instantaneous crystallinity at 5-15 mins ($X_i = 4.89 \pm 1.84\%$).....	31
18	Crystallization of native PHB granules dehydrated by freeze-drying (blue) and acetone extraction (red)	32
19	PHB granules heated at 120°C in acidic solution (pH 2): (a) relative molecular weight and PHB content versus exposure time; (b) TEM image of granules at 120°C for 1 hr.....	33
20	ATR-FTIR measurements for heated PHB granules (120°C, 1 hr) in acidic solution (pH 2): (a) time development of the infrared absorption spectra; (b) <i>in situ</i> crystallinity versus measurement time, illustrating the instantaneous crystallinity at 15-60 mins ($X_i = 22.52 \pm 2.43\%$).....	34
21	Crystallization of PHB granules heated at 80-140°C over 4 hrs	35
22	Log-log plot illustrating the linearity of <i>in situ</i> crystallization versus time of heated PHB granules	35
23	Crystallization growth rate parameter k as a function of temperature for heated PHB granules	36
24	PHB granules in alkaline solution (pH 12) at room temperature: (a) relative molecular weight and PHB content versus exposure time; (b) TEM image of granules at pH 12 for 1 hr	37
25	ATR-FTIR measurements for alkaline PHB granules (pH 12, 1 hr): (a) time development of the infrared absorption spectra; (b) <i>in situ</i> crystallinity versus measurement time, illustrating the instantaneous crystallinity at 3-5 mins ($X_i = 40.59 \pm 1.92\%$)	38
26	Crystallization of PHB granules with varying pH over 4 hrs.....	39
27	Log plot illustrating the linearity of <i>in situ</i> crystallization versus pOH of alkaline PHB granules	40
28	Illustrations of PHB crystallization: (a) <i>pure PHB</i> , spherulitic crystal growth from infinitesimal point source nuclei; (b) <i>heated PHB granules</i> , moderate granule aggregation and random crystal growth where intra-granule water and membranes are displaced; (c) <i>alkaline PHB granules</i> , instant crystal growth inward from granule surfaces lacking membranes.....	41
29	Free energy versus cluster radius for homogeneous (solid line) and heterogeneous (dotted line) nucleation, where ΔG is the total Gibbs free energy, ΔG_s is the surface energy component, ΔG_v is the volume energy component (dashed line), r_{cr} is the critical radius (primed values indicate parameters associated with a lowered free energy barrier due to heterogeneous nucleation) [20, 32]	42
30	Crystallization of PHB granules centrifuged at 1250-10000 g over 1 hr	46
31	SEM images of cells: (a) before centrifugation; (b) after centrifugation at 5000 g for 30 min... ..	47

32	Ultrasonicated PHB granules at 22.5 kHz: (a) relative molecular weight and <i>in situ</i> crystallinity versus energy input; (b) TEM image of native granules ultrasonicated at 4.5 kJ/mL.....	47
33	ATR-FTIR spectral background interference of non-PHB biomass, water, and 50 g/L SDS	48
34	TEM images of PHB granules treated with 50 g/L SDS	48
35	TEM images of PHB granules in varying environmental conditions arranged in order of increasing aggregation: (a) granules <i>in vivo</i> (pH 7); (b) native granules (pH 2); (c) alkaline granules (pH 12); (d) heated granules (120°C, 1 hr); (e) ultrasonicated granules (4.5 KJ/mL); (f) granules with surfactant (50 g/L SDS)	50
36	Molecular weight (solid lines) and <i>in situ</i> crystallinity (dashed lines) of heated granules (blue) and alkaline granules (red) over 4 hrs	51
37	Molecular weight (solid lines) and PHB content (dotted lines) of PHB-containing cells treated at room temperature in alkaline solution (pH 11) with an acid pretreatment (pH 2) at 100°C for 1hr (blue) and without an acid pretreatment (red)	54

LIST OF ABBREVIATIONS AND SYMBOLS

List of Abbreviations

PHA	Polyhydroxyalkanoate
PHB	Poly(3-hydroxybutyrate)
3HB	3-hydroxybutyrate
3HV	3-hydroxyvalerate
PHBV	Poly(3-hydroxybutyrate-co-3-hydroxyvalerate)
PHBVV	Poly(3-hydroxybutyrate-co-3-hydroxyvalerate-co-4-hydroxyvalerate)
HA	Hydroxyalkanoate
XRD	X-Ray Diffraction
DSC	Differential Scanning Calorimetry
ATR	Attenuated Total Reflectance
FTIR	Fourier Transform Infrared
ATR-FTIR	Attenuated Total Reflectance Fourier Transform Infrared Spectroscopy
EM	Electron Microscopy
TEM	Transmission Electron Microscopy
SEM	Scanning Electron Microscopy
H ₂ SO ₄	Sulfuric Acid
NaOH	Sodium Hydroxide
SDS	Sodium Dodecyl Sulfate
AVG	Average
STD	Standard Deviation

List of Symbols

X	Crystallinity	c	Speed of light (299,792,458 m/sec)
X_i	<i>In situ</i> crystallinity	k_B	Boltzmann constant (1.381×10^{-23} J/K)
t	Time	R	Gas constant (8.314 J/K·mol)
T	Temperature	h	Planck's constant (6.626×10^{-34} J·sec)
n	Avrami exponent	M_v	Viscosity-average molecular weight
k	Growth rate parameter	M_v^0	Original molecular weight
k_o	Pre-exponential factor for k	η	Intrinsic viscosity
G	Spherulitic growth rate	K	Mark-Houwink-Sakurada constant
G_o	Pre-exponential factor for G	a	Mark-Houwink-Sakurada exponent
ΔG	Free-energy	d	Depth of penetration
ΔG_v	Volumetric free-energy	n_1	Refractive index of ATR-crystal
ΔG_s	Surface free-energy	n_2	Refractive index of sample
σ	Surface energy	n_{21}	Refractive index ratio n_2/n_1
ΔE_n	Energy required for nucleation	θ	Angle of incidence
ΔE_g	Energy required for crystal growth	x	Displacement
ΔE_a	Activation energy	x_{eq}	Equilibrium distance
E	Vibrational energy	m_j	Mass of component j
$\tilde{\nu}$	Wavenumber	μ	Reduced mass
f	Frequency	k_s	Force constant
λ	Wavelength	w	Size parameter
I	Signal intensity	L	Characteristic crystal length
I_0	Source intensity	r	Radius
\mathcal{T}	Transmittance	r_n	Nucleus radius
A	Absorption	r_s	Spherulite radius
$A_{\tilde{\nu}}$	Absorption	r_{cr}	Critical radius for nucleation
$A_{m \tilde{\nu}}$	Absorption of component m at $\tilde{\nu}$	a	Surface shape factor
$AI_{\tilde{\nu}}$	Absorption index at $\tilde{\nu}$	ϕ	Volumetric shape factor
AI_i	Instantaneous absorption index	m	Slope of ATR-FTIR/DSC correlation
ΔH_m	Enthalpy of melting	b	Intercept of ATR-FTIR/DSC correlation
T_m	Melting Point		

CHAPTER 1

INTRODUCTION

1.1 Bioplastics and Polyhydroxyalkanoates (PHA)

With the widespread use of plastics and growing environmental awareness, much attention is being turned to bioplastics as eco-friendly alternatives to petroleum-based plastics. Plastics are regularly used in a plethora of industrial, commercial, and domestic applications because of their high strength, elasticity and durability, light weight, low cost, favorable thermal and optical properties. Today, most common plastics are non-biodegradable, synthetic polymers derived from petrochemical feedstocks. And, according to the United States Energy Information Administration, the U.S. has consumed over three billion barrels of crude oil for the production of petrochemical feedstocks since 1995 [1]. This accounts for approximately 4% of total US oil consumption [1]. Moreover, non-biodegradable plastics present waste management problems because many applications include short-lived, disposable products, such as films and coated paper products, packaging materials and bags, cosmetics and food servicing products [2]. Bioplastics, on the other hand, are completely biodegradable and can be derived from renewable feedstocks and/or agricultural byproducts.

Polyhydroxyalkanoate (PHA) is a class of naturally occurring biopolymers synthesized and stored in microbial cells (see Figure 1) as carbon and energy reserves, similar to the synthesis and storage of fat in humans [2]. Bioplastics made from PHA may serve as environmentally friendly substitutes for petroleum-based plastics because PHA is biodegradable and derived from renewable resources [2, 3]. PHA has similar material properties to many petroleum-based polymers and it can be processed on much of the same equipment [3-5]. In the market, however, PHA is limited due to high production costs.

In commercial production, microbial cells are grown in aqueous media and PHA accumulates as tiny granules inside the cells (see Figure 1) [2-6]. Following growth, the PHA granules must be separated from the cells and purified. During extraction, the environment of the granules changes and may cause the PHA to crystallize [3, 6]. This research focuses on the crystallization of PHA granules in different environmental conditions. Understanding this type of material transformation may help to improve PHA production and reduce the cost of bioplastics.

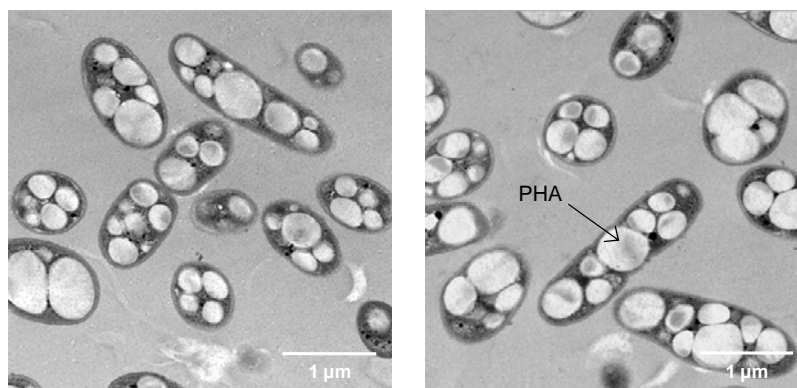


Figure 1. TEM images of microbial cells containing PHA granules

1.2 Poly(3-hydroxybutyrate) (PHB)

The focus of this research is the most widely studied form of PHA, poly(3-hydroxybutyrate) (PHB), a homopolymer of the monomer 3-hydroxybutyrate (3HB). Another common monomer of PHA is 3-hydroxyvalerate (3HV). Together, 3HB and 3HV may constitute a copolymer of poly(3-hydroxybutyrate-*co*-3-hydroxyvalerate) (PHBV), which is known to be tougher and less brittle than PHB [3, 5, 7]. Figure 2 illustrates the general chemical structures of PHA, PHB, PHV, and PHBV [8]. A variety of forms of PHA exist where the side group (R) may be aliphatic or aromatic, and vary in degree of saturation and branching [8]. PHB, for instance, has a methyl side group ($-\text{CH}_3$), while PHV has a larger ethyl side group ($-\text{CH}_2-\text{CH}_3$). Copolymers with varying fractions of HB, HV, and/or other hydroxyalkanoic (HA) monomers can be biologically engineered to exhibit more favorable mechanical and thermal properties (see Table 1) [2-5].

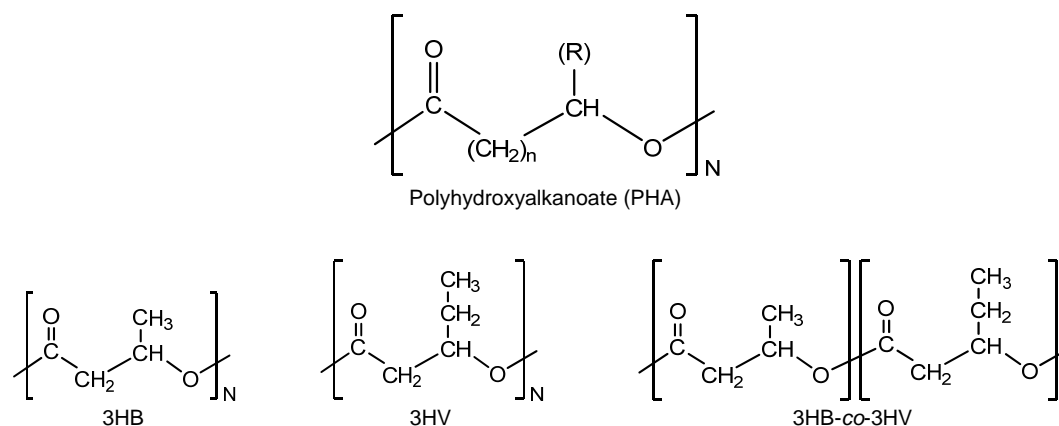


Figure 2. General chemical structure of polyhydroxyalkanoates, the monomers 3HB and 3HV, and a copolymer 3HB-*co*-3HV [8]

Table 1. Typical material properties of PHBV with varying fractions of 3HV [2]

Property	3HV fraction, mol%		
	0	10	20
Crystallinity (%)	80	60	35
Melting point (°C)	177	140	130
Tensile strength (MPa)	40	25	20
Flexural modulus (GPa)	3.5	1.2	0.8
Elongation to break (%)	8	20	50
Impact strength (J/m)	60	110	350

In addition to chemical composition, other properties of PHB, including molecular weight and crystallinity, play a significant role in the resulting material properties. PHB is a high molecular weight polymer ranging from 2×10^5 to 3×10^6 Daltons, depending on cell growth and polymer extraction [9]. As a general rule, high molecular weight or long chain polymers yield more desirable material properties (i.e., elastic modulus, tensile strength, melting point, etc.) because the degree of intermolecular entanglement increases with molecular weight [10, 11]. If the molecules are reduced in size, however, due to thermal, chemical, or enzymatic degradation, the degree of entanglement decreases and the resulting material properties may deteriorate.

The manner in which molecules align themselves into well-ordered structural domains is known as crystallinity, ranging from amorphous (0%) to crystalline (100%) [10, 11]. Materials composed of small molecules, such as water, are often fully amorphous (i.e., liquid state) or fully crystalline (i.e., solid state) [11]. Long chain polymers, on the other hand, are never purely crystalline (ranging from 0-95%) [11]. Purified PHB is a semi-crystalline material (50-80%) [12-14]. When PHB is heated above its melting point ($\sim 180^\circ\text{C}$), however, it becomes a fully amorphous melt (0%) [12-14]. Upon cooling, the PHB molecules crystallize, forming regions of crystalline and amorphous phases as shown in Figure 3 [10, 11, 15-17]. As illustrated, the amorphous regions are unordered, fluid-like entanglements of loosely packed molecules, while the crystalline regions are arranged into tightly packed helical chains [10, 11]. The unique elastic behavior of PHB and other semi-crystalline polymers is attributed to the random occurrence of amorphous and crystalline phases throughout the material [11]. Amorphous regions are highly mobile, free to stretch and bend, making plastics more flexible and elastic. Crystalline regions,

on the other hand, are quite rigid, giving plastics their high strength and durability. Highly crystalline materials such as PHB (50-80%) tend to be very brittle and inflexible, while lower crystalline materials such as PHBV (30-60%) are tougher and more elastic (see Table 1) [2-5].

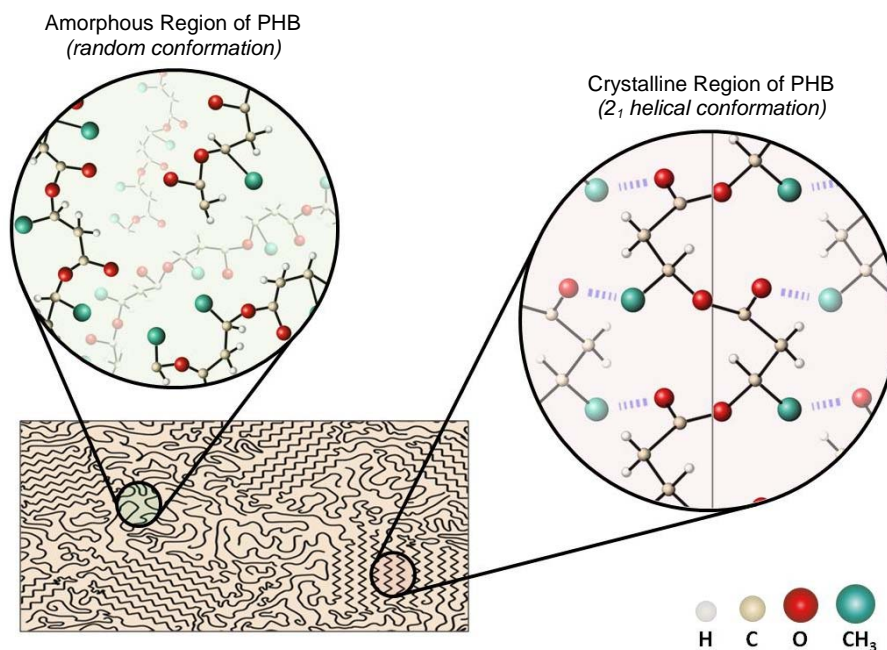


Figure 3. Amorphous and crystalline regions of a semi-crystalline polymer such as PHB [10, 11, 15-17]

The proposed crystal structure of PHB consists of two antiparallel, left-handed 2_1 -helices (see Figure 3) [15-17]. The driving force behind this energetically favorable structure is thought to be C–H \cdots O hydrogen bonding between the carbonyl (C=O) and methyl (CH₃) groups in PHB [17-19]. Referring to Table 1 and Figure 2, it becomes clear that the length of the side chain (R) is one of several factors that directly affect polymer crystallinity [2-5, 10, 11]. That is, PHB has a short side chain (–CH₃) and easily conforms to a helix as shown in Figure 3. In the case of PHBV, however, some fraction of the side chains may be longer (–CH₂–CH₃) disrupting the tightness of the helical conformation, thereby lowering the crystallinity.

Other factors that may affect polymer crystallinity can be classified as external, mechanical, or thermal [11, 20]. External factors include chemical potential (pH), particle volume, molecular weight, and foreign environmental substances such as plasticizers or inhibitors. Mechanical factors depend on internal forces such as pressure or stress, and the

internal energy related to amorphous mobility, nucleation, crystal growth, and intra- and intermolecular bonding. Thermal factors are influenced by the temperature, entropy, and enthalpy of the system.

1.3 PHB Granules

In contrast to pure PHB, native PHB granules *in vivo* are fully amorphous, contain a small amount of water (5-10%), and are surrounded by a monolayer membrane composed of phospholipids and proteins [3, 6, 21-23]. Figure 4 shows a TEM image and schematic of a native PHB granule *in vivo*, illustrating the bilayer membrane surrounding the cells and the monolayer membrane surrounding each granule [3, 6, 21-23]. PHB is hydrophobic, or immiscible with water [21]. Hence, the granule membrane lipids are oriented with hydrophobic tails facing the PHB core and hydrophilic heads facing the outer surface cytosol [21, 22]. Two types of proteins associated with the granule membranes are enzymatic and structural. Enzymatic proteins include polymer synthases and depolymerases, responsible for the synthesis and breakdown of PHB respectively [21, 22]. Structural proteins, known as phasins, are non-enzymatic proteins, and may play a role in regulating or stabilizing the amorphous granules [21-24].

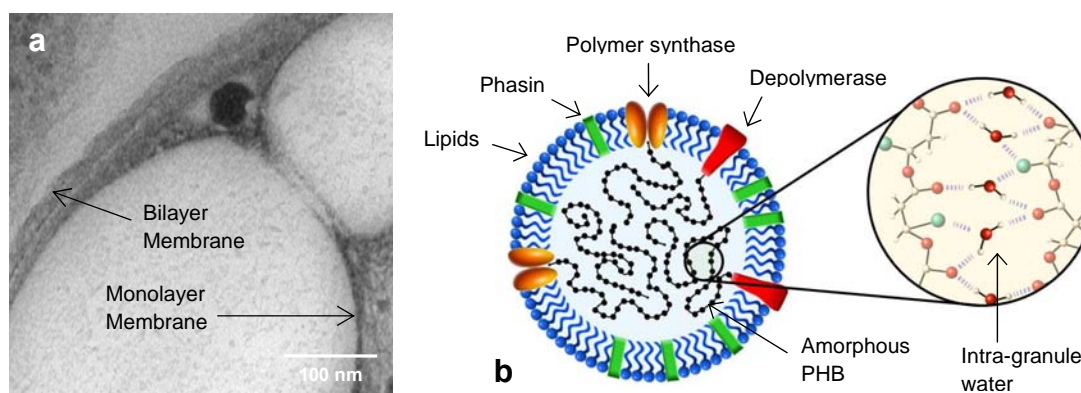


Figure 4. (a) TEM image of native PHB granules in microbial cells, illustrating the bilayer membrane surrounding each cell and the monolayer membrane surrounding each granule; (b) schematic of a native PHB granule, illustrating the intra-granule water, membrane lipids and proteins [3, 6, 21-23]

The amorphousness of native PHB granules is likely stabilized by the monolayer membrane surrounding the granules and intra-granule water [3, 6, 23]. *In vivo*, PHB must exist in

an amorphous state so that the cells can breakdown and consume PHB energy reserves for new cell growth and cell maintenance [3, 6]. In other words, highly crystalline PHB is too energetically stable for intracellular enzymes to effectively utilize [3, 6]. The 5-10% of water present in the granules is thought to act as a plasticizer, forming hydrogen bonds with the methyl and carbonyl groups of the polyester backbones in PHB (see Figure 4) [23]. This phenomenon may prevent strong intra- and intermolecular interactions from occurring between the C=O and CH₃ groups in PHB, thereby disrupting crystallization of the polymers [23].

During PHB extraction and purification, various physical and chemical treatments (e.g., heat, pH, centrifugation, ultrasonication, and surfactant) may be used to separate and purify the granules [25-28]. As a result, the aqueous environment of the cells changes and the PHB granules may undergo varying degrees of crystallization [22, 23, 29], as well as molecule degradation and morphological changes. Still, little is known about the *in situ* crystallization of PHB granules and how it may relate to material properties such as molecular weight and granule morphology.

1.4 Monitoring PHB Crystallization with ATR-FTIR

There are several methods to measure polymer crystallinity. Popular methods include: x-ray diffraction (XRD), differential scanning calorimetry (DSC), and attenuated total reflectance Fourier transform infrared spectroscopy (ATR-FTIR) [12-14, 30]. Monitoring the *in situ* crystallinity of PHB in its native aqueous environment, however, is difficult via XRD and DSC because of demands on material purity and dryness. ATR-FTIR is particularly useful for *in situ* measurements because no such sample preparation is necessary [30, 31]. That is, the infrared absorption spectra of PHB-containing cells in an aqueous solution can be measured directly to determine the true, *in situ* crystallinity of the native PHB granules without purifying or drying the PHB.

ATR-FTIR is an efficient analytical tool used to measure the chemical composition and structural arrangement of local molecular environments within solid, liquid, gas, semi-solid, and polymeric samples [30, 31]. When infrared light interacts with a polymer, infrared radiation is absorbed causing molecular vibrations at wavenumbers specific to its chemical bonds. In polyesters, for instance, two spectral regions are characteristic. The carbonyl group (C=O)

absorbs infrared light around $1800\text{-}1600\text{ cm}^{-1}$ and the ester backbone (C–O–C) absorbs infrared light around $1300\text{-}1000\text{ cm}^{-1}$ [30]. Figure 5 shows some typical vibrational modes associated with the chemical bonds present in PHB [30, 31]. Although the figure is not all inclusive, the basic stretching and bending vibrations shown are the primary focus of this research. Conformational changes in a sample, such as melting and crystallization, can be seen as an increase, decrease, or shift in the characteristic absorption bands of the infrared spectra [30, 31]. These spectral band changes reflect changes in the intensity and/or frequency of vibrational energy absorbed by the characteristic functional groups of a molecule [30, 31]. Intra- and intermolecular interactions, such as hydrogen bonding, may influence the type of vibration each functional group experiences. Consequently, the infrared spectrum of PHB is information rich, providing a quick and convenient method to monitor conformational changes in PHB, such as crystallization.

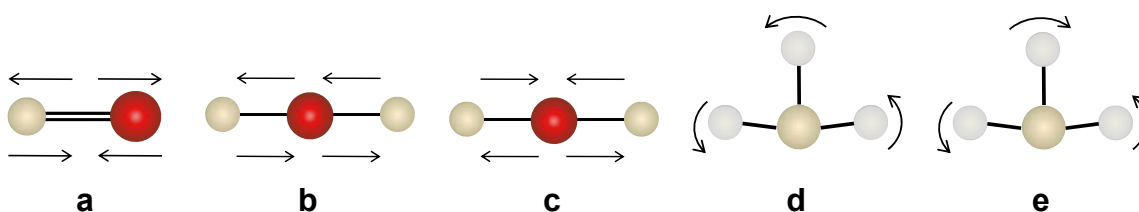


Figure 5. Some common vibrational modes associated with PHB: (a) C=O stretching; (b) C–O–C asymmetric stretching; (c) C–O–C symmetric stretching; (d) CH₃ symmetric bending; (e) CH₃ asymmetric bending [30, 31]

1.5 Modeling PHB Crystallization

The crystallization of PHB is an energetically favorable process that may be driven by its environment. Crystallization can be isothermal or non-isothermal and may depend on temperature, pH, external force, or environmental chemistry [20, 32]. Polymer crystallization begins as groups of molecules aggregate into tiny clusters forming nuclei [11, 20]. Then, sheet-like structures known as lamellae grow outward from the nuclei in the form of spherulites (see Figure 6) [11, 20].

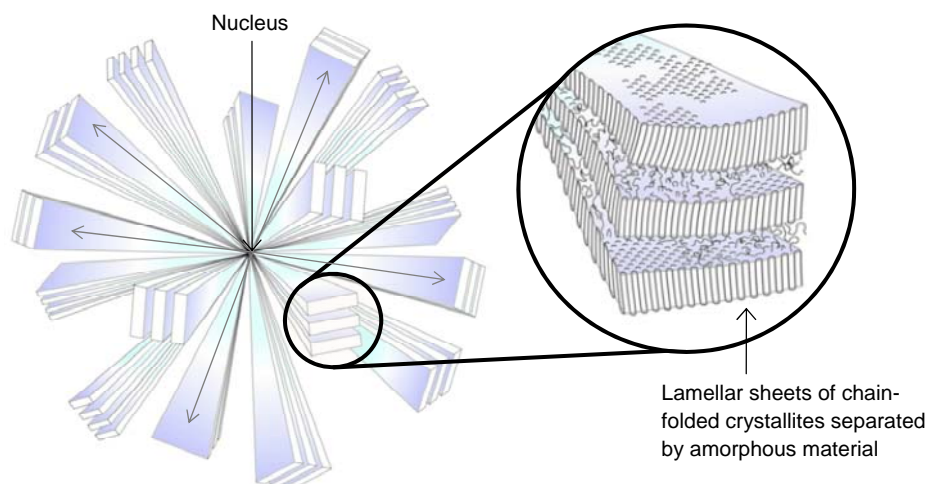


Figure 6. Schematic of a spherulite, illustrating the nucleus, lamellae, and direction of growth [11, 20]

Figure 7 shows the isothermal crystallization of PHBV from a melt at 100°C, illustrating nucleation and crystal growth. The extent of crystallization depends on the thermodynamics of phase separation (i.e., amorphous to crystalline) and the geometry of nuclei formation and spherulitic growth [11, 20, 32]. Nucleation is primarily driven by temperature and chemical potential, and occurs at a critical nucleus size where the free-energy barrier necessary for crystal growth is overcome [20, 32]. In PHB granules, different environmental factors such as temperature and pH may promote granule crystallization by lowering the free-energy barrier or increasing the number of nucleation sites. Other environmental factors, such as granule impurities (i.e., non-PHB biomass and water), external force and environmental chemistry, may promote/inhibit granule crystallization by changing the free-energy barrier or crystal geometry.

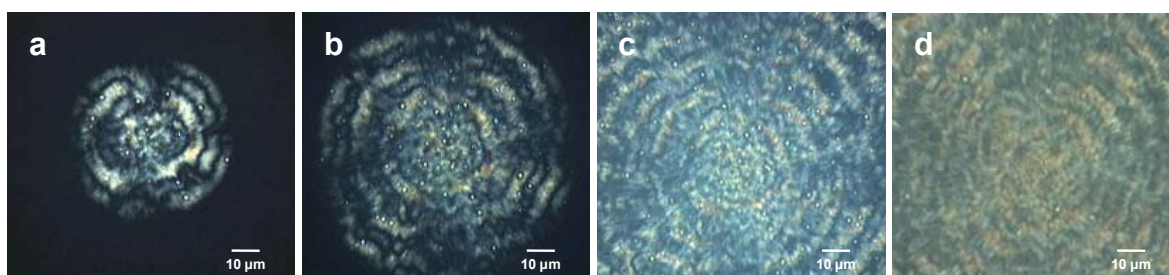


Figure 7. Crystallization of PHBV from melt at 100°C after (a) 3 min, (b) 7 min, (c) 15 min, and (d) 3 hr

In pure PHB, the crystallinity (X) is well described by Avrami's equation for isothermal crystallization [18, 33, 34]:

$$X = 1 - \exp[-k t^n] \quad (1)$$

where t is the crystallization time, k is a rate constant dependent on nuclei formation and polymer transport, and n is the Avrami exponent dependent on the nature of nucleation and the geometry of crystal growth. Another important quantity describing polymer crystallization (in general) is the spherulitic growth rate (G), which can be modeled by the Turnbull-Fisher expression [20, 35-37]:

$$G = G_o \exp \left[- \frac{(\Delta E_n + \Delta E_g)}{k_B T} \right] \quad (2)$$

where ΔE_n is the free-energy barrier required for nucleation, ΔE_g is the activation energy required for crystal growth (i.e., polymer chain folding and rearrangement), k_B is the Boltzmann constant, T is the isothermal crystallization temperature, and G_o is a pre-exponential factor. Analogous to the Turnbull-Fisher expression, the crystallization rate constant (k) in the Avrami equation may be expressed (in general) by a modified form of the Arrhenius equation [34, 36]:

$$k^{1/n} = k_o \exp \left[- \frac{\Delta E_a}{R T} \right] \quad (3)$$

where $\Delta E_a = (\Delta E_n + \Delta E_g)$ is the total crystallization activation energy (i.e., energy required to overcome the free-energy barrier), R is the gas constant, T is the isothermal crystallization temperature, n is Avrami's exponent, and k_o is a modified pre-exponential factor, independent of temperature.

1.6 Research Objective

The objective of this research is to observe and understand the *in situ* crystallization of native PHB granules in varying environmental conditions, which is quite different from the crystallization process of pure PHB. To understand these processes, it is important to identify the driving forces behind PHB crystallization and determine the environmental factors present in native PHB granules that may inhibit their crystallization *in vivo*. When the crystallization factors of pure PHB are compared with those of native PHB granules, possible inhibitors and physical

properties, such as the granule membrane, intra-granule water, molecular weight and granule morphology, seem most likely to alter nucleation, crystal growth, and spherulitic geometry.

The approach of this work is to develop a general empirical model, analogous to those above (Eqn 1-3), describing the *in situ* crystallization of native PHB granules in different environmental conditions (i.e., heat, pH, centrifugation, ultrasonication, and surfactant). The foundation of the empirical model will be built from crystallinity measurements of native PHB granules in aqueous solution with ATR-FTIR spectroscopy. Modified parameters that arise in the model, such as rate constants and exponents, will link the various environmental conditions to the specific driving forces and inhibitors present in the crystallization processes. Also, viscosity-average molecular weight (M_v) measurements and electron microscopy (EM) images of the PHB granules will be used to explain the influence of PHB crystallinity on molecule degradation and granule morphology. Such a model may serve as a useful tool in the development of more economical production methods and useful applications of PHB, as well as, increase knowledge pertaining to the mechanisms associated with biopolymer production and degradation.

CHAPTER 2

MATERIALS AND METHODS

2.1 PHB Granules

In this work, *Ralstonia eutropha* cells containing 60-70 wt% PHB were stored at room temperature ($\sim 20^{\circ}\text{C}$) in solutions of 0.2 M sulfuric acid (H_2SO_4) as three different slurries of 150-250 g cell mass/L (refer to Sec 4.2 Table 4). Several aqueous solutions of PHB-containing cells were prepared for controlled samples of different crystallinity:

- (a) *Native PHB granules*, suspended in acidic solution (pH 2) as described above;
- (b) *Heated PHB granules*, where 3-5 mL of the native granules were heated in glass test tubes at $80\text{-}140^{\circ}\text{C}$ and maintained for 0-4 hr;
- (c) *Alkaline PHB granules*, where the pH of the native granules was increased up to 12 by adding equal volumes (3-5 mL) of varying concentrations of sodium hydroxide (NaOH) to the native granules at room temperature;
- (d) *Centrifuged PHB granules*, where 3-5 mL of the native granules were spun at 10000 g for 0-1 hr at room temperature;
- (e) *Ultrasonicated PHB granules*, where 10 mL of the native granules were ultrasonicated at a constant frequency of 22.5 kHz with 0-300 J/mL for three cycles of 10 sec on, 20 sec off to control the samples at room temperature;
- (f) *PHB granules with surfactant*, where 0-50 g/L sodium dodecyl sulfate (SDS) was added to 3-5 mL of the native granules at room temperature.

2.2 Purified PHA

Pure PHA samples (PHB film, PHB powder, and poly(3-hydroxybutyrate-*co*-3-hydroxyvalerate-*co*-4-hydroxyvalerate) (PHBVV) film) were prepared from various cell slurries (not discussed in this work), and used as standards of different crystallinity in the DSC analysis.

For preparation of pure PHB, the microbial cells were freeze dried, dissolved in hot chloroform, and filtered to separate the polymer solution from the residual non-PHB biomass. Pure PHB was precipitated from the chloroform solution by adding hexanes, filtered and dried.

The purified PHB was then dissolved in hot chloroform and cast on a clean glass surface as a thin film (~0.2 mm). The non-PHB biomass leftover from solvent extraction was oven dried at 60°C and saved for later use.

2.3 Chemical Analysis

The different aqueous solutions of PHB granules described above were centrifuged at 7500 g for 10 min to separate the soluble solids in the supernatant (i.e., dissolved biomass) from the insoluble solids in the pellet (i.e., intact biomass and PHB granules). The dissolution of proteins (i.e., soluble solids) released from damaged cells was measured at 595 nm with a UV/Vis spectrophotometer (Beckman Coulter DU530, Fullerton, CA) and Bradford assay [38]. The PHB content of the microbial cells (i.e., insoluble solids) was determined via acid-catalyzed methanolysis of the biopolyesters in methanol (3 wt% H₂SO₄) at 100°C for 8-10 hr [39]. The resulting 3-hydroxybutyric methyl ester was hydrolyzed into 3-hydroxybutyric acid at pH 11 with 10 N NaOH. The liquid samples were analyzed at 210 nm using an HPLC equipped with a UV detector (Shimazu, Japan) and an organic acid column (OA-1000, Alltech, Deerfield, IL) maintained at 65°C and eluted with a sulfuric acid solution (pH 2) at 0.8 mL/min.

2.4 ATR-FTIR Spectroscopy

The infrared absorption spectra of PHB-containing cells, pure PHA samples, non-PHB biomass, and water were recorded with a Nicolet Avatar 370 FTIR spectrometer (Thermo Electron Co., Madison, WI). All measurements were taken in ambient conditions on a germanium crystal window of micro-horizontal attenuated total reflectance (ATR). A total of 32 scans were averaged for measurement of a single sample over 1 min.

For time-resolved measurements describing the crystallization of pure PHB, the sample was melted at 180°C, placed directly on the ATR window, and allowed to cool at room temperature. Absorption spectra were collected every 1-2 min over the duration (30-60 min) of the process.

For *in situ* measurements of the PHB-containing cells, a small drop (~2 µL) of aqueous solution was placed directly on the ATR window and allowed to evaporate. During water

evaporation, the PHB-containing cells deposited onto the window via sedimentation and absorption spectra were collected every 1-2 min for the duration (30-60 min) of the process.

2.5 Differential Scanning Calorimetry (DSC)

Thermal properties of pure PHA samples were examined via differential scanning calorimetry (DSC). A Modulated 2920 instrument (TA Instruments, New Castle, DE) equipped with a refrigerated cooling system was run in a heat-cool-heat cycle at a rate of 5°C /min in nitrogen. The selected temperature range was 30-210°C with sample weights of 4.5-5.5 mg.

2.6 Viscosity-average Molecular Weight

To measure molecular weight, PHB was extracted from the cells in hot chloroform. An Ubbelohde OC viscometer (Technical Glass Products Inc., Dover, NJ) immersed in a water bath at 30°C was used to measure the intrinsic viscosity η of the PHB-chloroform solutions. The viscosity-average molecular weight M_v of PHB was calculated according to the Mark-Houwink-Sakurada equation:

$$\eta = K (M_v)^a \quad (4)$$

where $K = 7.7 \times 10^{-5}$ dL/g and $a = 0.82$ are constants describing the PHB-chloroform properties [40]. The relative molecular weight was calculated as follows:

$$M_v/M_v^0 \quad (5)$$

where M_v^0 is the original viscosity-average molecular weight of the native PHB granules before treatment, measured according to equation 4.

2.7 Transmission Electron Microscopy (TEM)

The transmission electron microscopy (TEM) images were viewed on a LEO 912 EFTEM (Zeiss, Germany) at 100 kV and photographed with a frame-transfer CCD camera (Proscan, Germany). The cells were fixed with glutaraldehyde and calcium chloride in a sodium cacodylate buffer, then post-fixed with osmium tetroxide, stained with uranyl acetate, dehydrated with

ethanol and embedded in epoxy. Ultrathin (60-80 nm) sections were obtained on an Ultracut E ultramicrotome (Reichert, Austria), double stained with uranyl acetate and lead citrate.

2.8 Scanning Electron Microscopy (SEM)

The scanning electron microscopy (SEM) images were captured at a resolution of 2560 x 1920 with a Hitachi S-4800 field emission scanning electron microscope (FESEM) (Hitachi High-Technologies Corp., Japan). The cells were freeze-dried for 3-4 hours, mounted on aluminum stubs with double-sided conductive tape, and coated with 3 nm gold/palladium in a Hummer 6.2 sputter coater (Anatech Ltd., Union City, CA) before viewing.

CHAPTER 3

MONITORING PHB CRYSTALLIZATION WITH ATR-FTIR

Attenuated total reflectance Fourier transform infrared spectroscopy (ATR-FTIR) is a quick and convenient method to monitor the crystallization of PHB, in both its purified form *in vitro* and its native form *in vivo*. Unlike purified PHB, the amorphousness of PHB granules *in vivo* may be stabilized by proteins, lipids, and water [6, 23, 29]. When monitoring the infrared absorption spectra of PHB-containing cells in an aqueous solution, these impurities (i.e., non-PHB biomass and water) may generate considerable background noise and spectral interference. Moreover, evaporation of water during the measurement may cause the granules to crystallize. Hence, the absorption spectra may not reflect the true, instantaneous crystallinity of PHB *in vivo*.

In this work, we developed the first known method to monitor the instantaneous crystallinity of PHB granules in microbial cells suspended in an aqueous solution of varying environmental conditions. Spectral interference from background absorptions caused by water and other non-PHB cellular components were measured and accounted for in the measurements at specific wavenumbers. The following sections (Sec 3.3-6) describe the *in situ* method and provide a quantitative description of PHB crystallinity by correlating ATR-FTIR measurements with DSC results.

3.1 Fourier Transform Infrared Spectroscopy (FTIR) and Attenuated Total Reflectance (ATR)

In Fourier transform infrared spectroscopy (FTIR), infrared radiation is emitted from a heat source containing all of the wavenumbers over the mid-infrared spectrum ($\tilde{\nu} = 4000\text{-}400\text{ cm}^{-1}$) and propagated through an interferometer, before entering a sample of interest [31]. The wavenumber associated with monochromatic radiation is proportional to its frequency [30, 31]:

$$\tilde{\nu} = f/c \quad (6)$$

where $\tilde{\nu}$ is the wavenumber in cm^{-1} , c is the speed of light in vacuum ($2.99792458 \times 10^{10}$ cm/sec), and f is the frequency of radiation in sec^{-1} , which is inversely proportional to its wavelength λ :

$$f = c/\lambda. \quad (7)$$

To analyze a sample via FTIR, a spectrum of infrared radiation is propagated through the sample and the transmittance of radiation from the sample is measured. The transmittance is [30, 31]:

$$\mathcal{T} = I/I_0 \quad (8)$$

where I_0 is the intensity of infrared radiation entering the sample (i.e., source) and I is the intensity transmitted (i.e., signal). Alternatively, the absorption of infrared radiation by the sample is measured according to Beer's law [30, 31]:

$$A = -\log\left(\frac{I}{I_0}\right). \quad (9)$$

The term *Fourier transform* refers to the mathematical algorithm used to convert the raw infrared signal in the time domain into a transmittance/absorption spectrum in the frequency domain [31].

Attenuated total reflectance (ATR) is a slightly different technique to that described above. Instead of transmitting infrared radiation through a sample, a sample is placed in contact with a material of high refractive index (e.g., ATR crystal), and an evanescent wave is internally reflected across the interface of the media (see Figure 8) [31]. The less dense sample absorbs radiation at the point(s) of reflection. The unabsorbed, reflected radiation is measured by a detector. The intensity of the radiation absorbed by the sample decays exponentially with the depth of penetration, defined as [31]:

$$d = \frac{\lambda}{2\pi n_1 \sqrt{\sin^2 \theta - n_{21}^2}} \quad (10)$$

where λ is the wavelength of infrared radiation, θ is the angle of incidence, n_1 is the refractive index of the ATR crystal, n_2 is the refractive index of the sample, and $n_{21} = n_2/n_1$ where $n_2 < n_1$. Depending on the angle of incidence, the evanescent wave may be internally reflected multiple times across the interface. Figure 8 illustrates the case of single internal reflection. An infrared absorption spectrum is obtained by ATR using the principles described above, so that:

$$A = -\log\left(\frac{I}{I_0}\right)$$

where I_0 is the intensity of radiation entering the ATR crystal (i.e., source) and I is the intensity of the internally reflected radiation (i.e., signal).

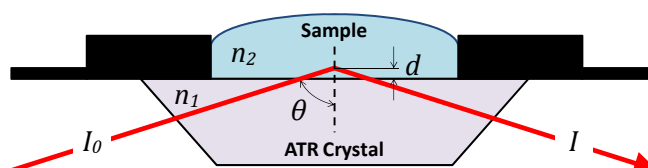


Figure 8. Schematic of attenuated total reflectance with single internal reflection [31]

Attenuated total reflectance Fourier transform infrared spectroscopy (ATR-FTIR) is particularly suited to measure samples too thick or complex for transmission spectroscopy [31]. Liquid mixtures, such as the aqueous solutions of PHB granules, can be conveniently analyzed via ATR-FTIR because the absorption spectra of each component are assumed unique and can be removed from the total spectrum by a technique known as spectral subtraction [30].

3.2 Molecular Vibrational Energy

In this work, the infrared absorption spectrum – a plot of the infrared absorption (A) versus wavenumber ($\tilde{\nu}$) – was analyzed to determine the amount of vibrational energy absorbed by the chemical bonds in PHB, and thereby determine its structural arrangement. The vibrational energy associated with the infrared spectrum is [30, 31]:

$$E = hc\tilde{\nu} \quad (11)$$

where E is the energy in Joules (J) and h is Planck's constant (6.626×10^{-34} J·sec). When a wide spectrum of infrared radiation propagates through a molecule, only radiation energy corresponding to the wavenumbers characteristic of the molecule's chemical bonds is absorbed. This absorbed energy may change the electronegativity or dipole moment of the chemical bonds, causing them to vibrate at frequencies equivalent to the radiation energy absorbed.

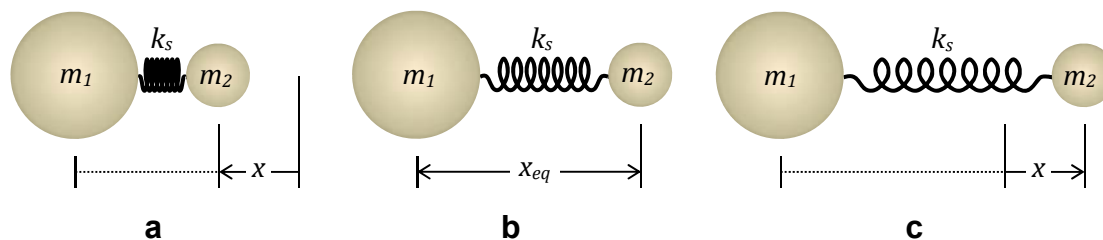


Figure 9. Simple harmonic oscillator: (a) compression ($x < 0$); (b) equilibrium ($x = 0$); (c) extension ($x > 0$)

Molecular vibrations are most conveniently modeled by classical mechanics as simple harmonic oscillations. Figure 9 illustrates a diatomic harmonic oscillator, where m_1 and m_2 , representing the masses of two atoms, are connected by a weightless elastic spring with a spring force constant k_s at an equilibrium distance x_{eq} [30, 31]. The differential equation of motion is [31]:

$$\mu \frac{d^2x}{dt^2} + k_s x = 0 \quad (12)$$

where d^2x/dt^2 is the second derivative of the displacement x with respect to time t , and μ is the reduced mass [31]:

$$\mu = \frac{m_1 m_2}{m_1 + m_2}. \quad (13)$$

Finally, solving the differential equation (12) yields an expression for the wavenumber in terms of the reduced molecular mass (μ) and the force constant associated with the chemical bond (k_s) [30, 31]:

$$\tilde{\nu} = \frac{1}{2\pi c} \sqrt{k_s/\mu}. \quad (14)$$

Equation 14 is used to determine the specific wavenumbers at which different chemical bonds will absorb infrared radiation. Based on this relationship, it is apparent that strong chemical bonds (i.e., large force constants) absorb infrared radiation at high wavenumbers, producing faster, high frequency vibrations [30]. Molecules of high molecular weight (i.e., reduced mass), on the other hand, absorb infrared radiation at low wavenumbers, producing slower, low frequency vibrations [30]. The infrared absorption spectrum characteristic of PHB is primarily focused around low wavenumbers ($1800\text{-}1000\text{ cm}^{-1}$), which is likely due to its high molecular weight.

3.3 Monitoring the Crystallization of Pure PHB with ATR-FTIR

Figure 10 shows a time development of the infrared absorption spectra illustrating the crystallization of pure PHB cooled from an amorphous melt at 180°C (solid line) to a semi-crystalline solid at room temperature (dashed line) over 45 min.

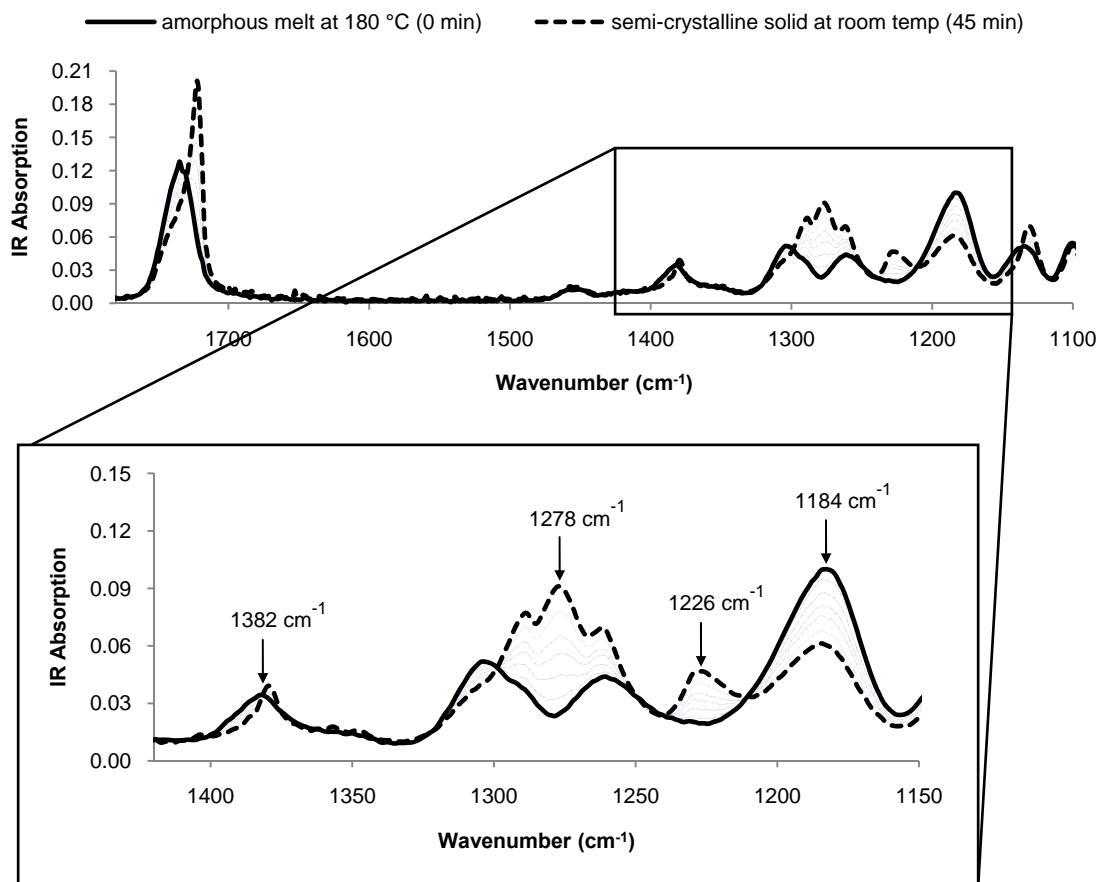


Figure 10. Time development of the infrared absorption spectra of pure PHB illustrating the crystallization due to cooling from an amorphous melt at 180°C (solid line) to a semi-crystalline solid at room temperature (dashed line) in ambient conditions

As seen in the figure, the absorption at 1184 cm^{-1} decreases with time, while the absorptions at 1226 and 1278 cm^{-1} increase with time. At 1382 cm^{-1} the absorption intensity does not change with time and is taken as the reference peak (discussed in more detail later) [41]. By scaling the absorptions measured at 1184, 1226, and 1278 cm^{-1} with the reference peak 1382 cm^{-1} , a value known as the absorption index ($AI_{\bar{\nu}}$) can be found using the equation:

$$AI_{\tilde{\nu}} = \frac{A_{\tilde{\nu}}}{A_{1382}} \quad (15)$$

where $A_{\tilde{\nu}}$ is the infrared absorption intensity measured at wavenumber $\tilde{\nu}$ and A_{1382} is the absorption intensity measured at the reference peak 1382 cm^{-1} .

The crystallization of pure PHB describing the material transition from an amorphous melt to a semi-crystalline solid has been studied by many research groups [12, 13, 16-18, 33, 42, 43]. When pure PHB is heated above its melting point ($\sim 180^\circ\text{C}$) it exists as an amorphous entanglement of loosely packed molecules [12]. Upon cooling, the PHB molecules crystallize, aligning into tightly packed helical chains, forming lamellar sheets and/or spherulites. [12]. Driven by C–H \cdots O hydrogen bonding between the carbonyl (C=O) and methyl (CH₃) groups in PHB, the molecular mobility of the PHB molecules becomes restricted due to chain folding and close packing into a crystalline state [17, 42, 43]. Conversely, melting PHB causes the C–H \cdots O hydrogen bonds to weaken, increasing molecular mobility.

The intra- and intermolecular bonds, such as hydrogen bonds, and the associated conformational changes that take place in PHB during crystallization can be monitored at specific wavenumbers of the infrared absorption spectra (see Figure 10) [14, 16-19, 33, 41-45]. The absorption band characteristic of the C=O stretching vibration, for instance, shifts from 1743 to 1722 cm^{-1} during crystallization, corresponding to a decreased dipole moment from the amorphous to crystalline phases of PHB, respectively [14, 16-19, 33, 42-45]. A comparable shift is seen at the wavenumber 1382 cm^{-1} , which corresponds to the CH₃ symmetric bending vibration [41]. These low-frequency shifts, along with several other spectral band changes, are likely due to the formation of C–H \cdots O hydrogen bonds during crystallization, which may reduce the vibrational freedom of the C=O and CH₃ groups in PHB [17-19, 42, 43]. In fact, the distance between the O atom of the C=O group and one of the H atoms of the CH₃ group in semi-crystalline PHB (2.63 \AA) is shorter than the van der Waals separation (2.72 \AA) [17, 43]. This suggests that C–H \cdots O hydrogen bonding must occur in PHB [43], and as a result, the C=O and CH₃ groups may vibrate in unison. Similarly, the backbone of the biopolyester undergoes conformational changes during crystallization. Of particular interest are the wavenumbers 1184 , 1226 , and 1278 cm^{-1} corresponding to the asymmetric stretching of the C–O–C backbone in the amorphous phase, the asymmetric stretching of the C–C–O bond in the crystalline phase due to

the formation of helical chains, and the CH₂ wagging of C–C–O backbone in the crystalline phase, respectively (see Figures 3 and 5) [14, 16-19, 33, 41, 44, 45].

The degree of crystallinity in PHB is commonly monitored relative to that of fully crystallized and amorphous PHB at the three representative wavenumbers 1184, 1226, and 1278 cm⁻¹ seen in Figure 10 [18, 33, 41]. As previously noted, the reference peak 1382 cm⁻¹ corresponds to the CH₃ group in PHB and undergoes a low-frequency shift similar to that of the C=O group. Although the reference peak experiences a small change in shape, the absorption intensity measured at 1382 cm⁻¹ is nearly constant, and is proportional to the concentration of PHB measured [41]. Furthermore, the small change of absorption intensity at 1382 cm⁻¹ is negligible when compared to the intensity changes that occur at 1184, 1226, and 1278 cm⁻¹. Therefore, the *absorption intensity* measured at 1382 cm⁻¹ can be considered insensitive to the degree of crystallinity, as previously stated by Bloembergen et al. [41]. Differences in PHB concentration during the measurement are accounted for by the absorption index (Eqn 15) discussed above.

3.4 ATR-FTIR/DSC Crystallinity Correlation

The absorption indices of amorphous PHB at 180°C (PHB melt) and three pure PHA samples (PHB film, PHB powder, and PHBVV film) were calculated from ATR-FTIR measurements as shown above from equation 15. The crystallinity (X) of the same three PHA samples were determined via DSC using the equation:

$$X = \frac{\Delta H_m}{\Delta H_{PHB}^0} \quad (16)$$

where ΔH_m is the enthalpy of melting of the sample and $\Delta H_{PHB}^0 = 146$ J/g is the theoretical enthalpy of melting of pure PHB crystals [12]. Figure 11 contains a plot of the crystallinity versus the absorption index of the PHA samples measured at wavenumbers 1184, 1226, and 1278 cm⁻¹. As seen in the figure, the crystallinity (X) is linearly correlated to the absorption index ($AI_{\bar{\nu}}$) following the empirical relation:

$$X = m(AI_{\bar{\nu}}) + b \quad (17)$$

where m is the slope and b is the intercept of the calibration lines. This correlation is reasonable because the absorption index is a measure of the number of molecules that are vibrating in the relative amorphous and crystalline phases, not a measure of the molecular concentration. That is, the degree of crystallinity is directly proportional to the fraction of molecules vibrating in the crystalline phase, which is directly measured by the absorption index.

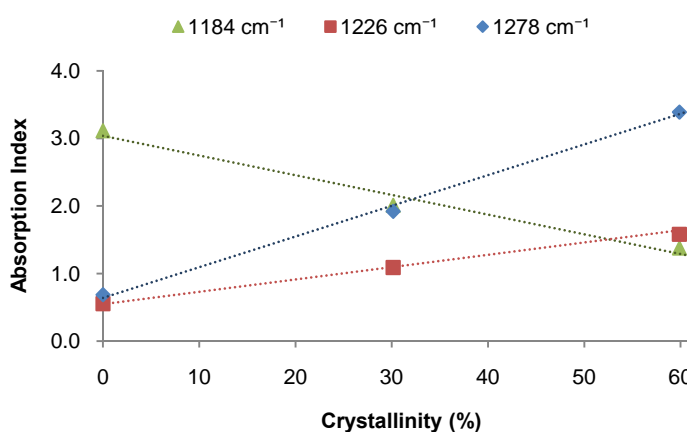


Figure 11. ATR-FTIR absorption index versus DSC crystallinity from pure PHA samples

Table 2 contains values of the absorption index ($AI_{\bar{\nu}}$), melting temperature (T_m), enthalpy of melting (ΔH_m), and crystallinity (X) for the pure PHA samples. Table 3 contains values of the slope (m), intercept (b), and correlation coefficient squared (R^2) at the wavenumbers 1184, 1226, and 1278 cm^{-1} , corresponding to equation 17.

Table 2. Infrared absorption indices, thermal properties, and crystallinity of pure PHA samples

Sample	AI_{1184}	AI_{1226}	AI_{1278}	T_m (°C)	ΔH_m (J g ⁻¹)	X (%)
PHB film	1.21	1.75	3.49	178.1	91.1	62.4
PHB powder	1.38	1.58	3.39	173.8	87.4	59.9
PHBVV film	2.01	1.09	1.92	97.4	44.0	30.1
PHB melt	3.11	0.55	0.69	--	--	0.0

Table 3. ATR-FTIR/DSC crystallinity correlation values

	1184 cm^{-1}	1226 cm^{-1}	1278 cm^{-1}
<i>m</i>	-2.91	1.82	4.54
<i>b</i>	3.04	0.55	0.64
R^2	0.9842	0.9915	0.9979

3.5 Monitoring the *In Situ* Crystallization of Native PHB Granules with ATR-FTIR

The native PHB-containing cells stored in acidic solution (pH 2) exhibited no biological activity. The mild acidic conditions caused some damage to the cell walls as seen in Figure 12, but did not significantly change the nature of the native PHB granules.

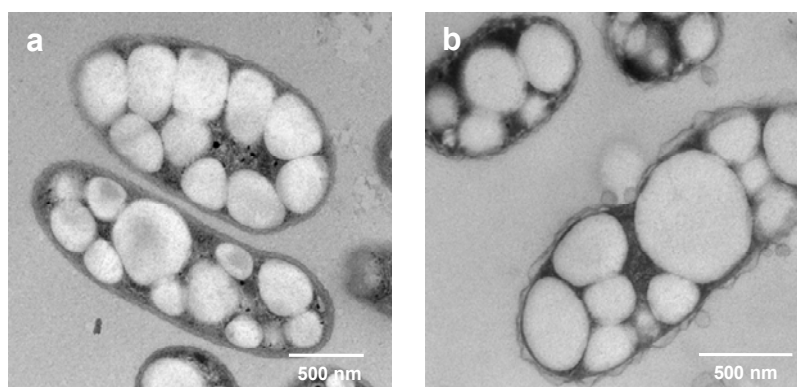


Figure 12. TEM images of PHB-containing cells: (a) in neutral solution (pH 7); (b) in acidic solution (pH 2)

Figure 13 shows a time development of the infrared absorption spectra of the native PHB granules in microbial cells suspended in acidic solution. In 30 min of measurement, a spectral pattern is observed that resembles the crystallization of pure PHB seen in Figure 10. Initially, the absorption spectrum of the solution is dominated by water (dotted line). As water evaporates in approximately 10 min, a secondary spectrum of the PHB granules and other cellular components emerges due to sedimentation (solid line). This spectrum may represent the true, instantaneous crystallinity of the native granules. After 30 min, the spectra changes due to excess dehydration, becoming fully developed, and may no longer represent the true, instantaneous crystallinity of the granules (dashed line).

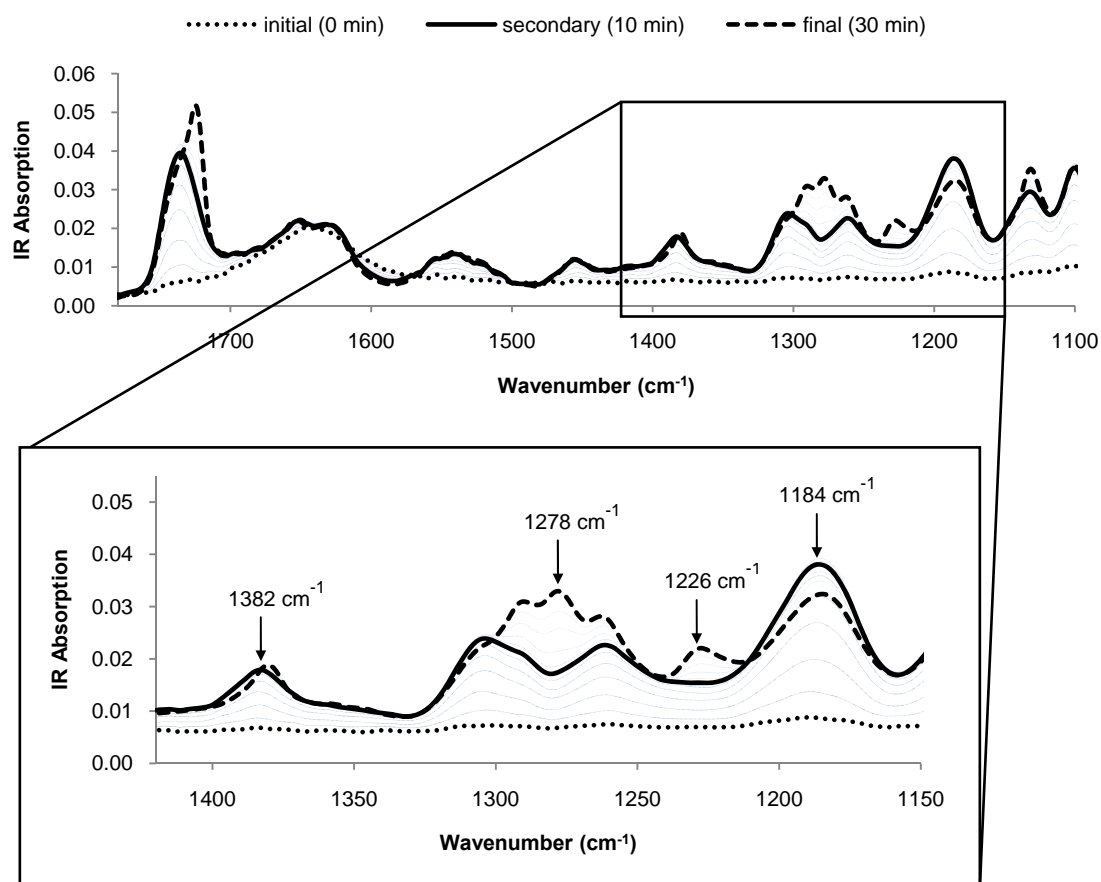


Figure 13. Time development of the infrared absorption spectra of PHB-containing cells suspended in acidic solution illustrating the initial spectrum dominated by water at 0 mins (dotted line), the secondary spectrum characteristic of the instantaneous crystallinity after 10 mins (solid line), and the final spectrum caused by extensive dehydration after 30 mins (dashed line)

According to water evaporation, the *in situ* measurements can be divided into three distinct stages. Figure 14 contains illustrations of the three stages (initial, secondary, and final) and a plot of the infrared absorption versus measurement time at the wavenumbers 1184, 1226, 1278, and 1382 cm^{-1} . Also shown in Figure 14 is data collected at the wavenumber 3414 cm^{-1} , an absorption band representative of O–H stretching present in water [30, 46]. The intensity at 3414 cm^{-1} can be used to estimate the relative fraction of water measured in the sample by scaling its absorbency to that of pure water. In stage 1 (0-5 min) the cells were initially suspended in water, and the infrared signal was predominated by water. As a result, very little, scattered absorption by the granules was observed. In stage 2 (5-15 min) the PHB-containing cells were settled down onto the ATR window and a stable region of the infrared

absorbencies reflecting the instantaneous crystallinity was observed. In stage 3 (15-30 min), excess dehydration of the PHB-containing cells caused the granules to further crystallize as seen by the divergence of infrared absorbencies measured at the representative wavenumbers. Obviously, the absorption measurements in the final stage do not reflect the true crystallinity of the native granules. In other words, the high crystallinity of the native granules in the final stage was artificially induced by excess dehydration.

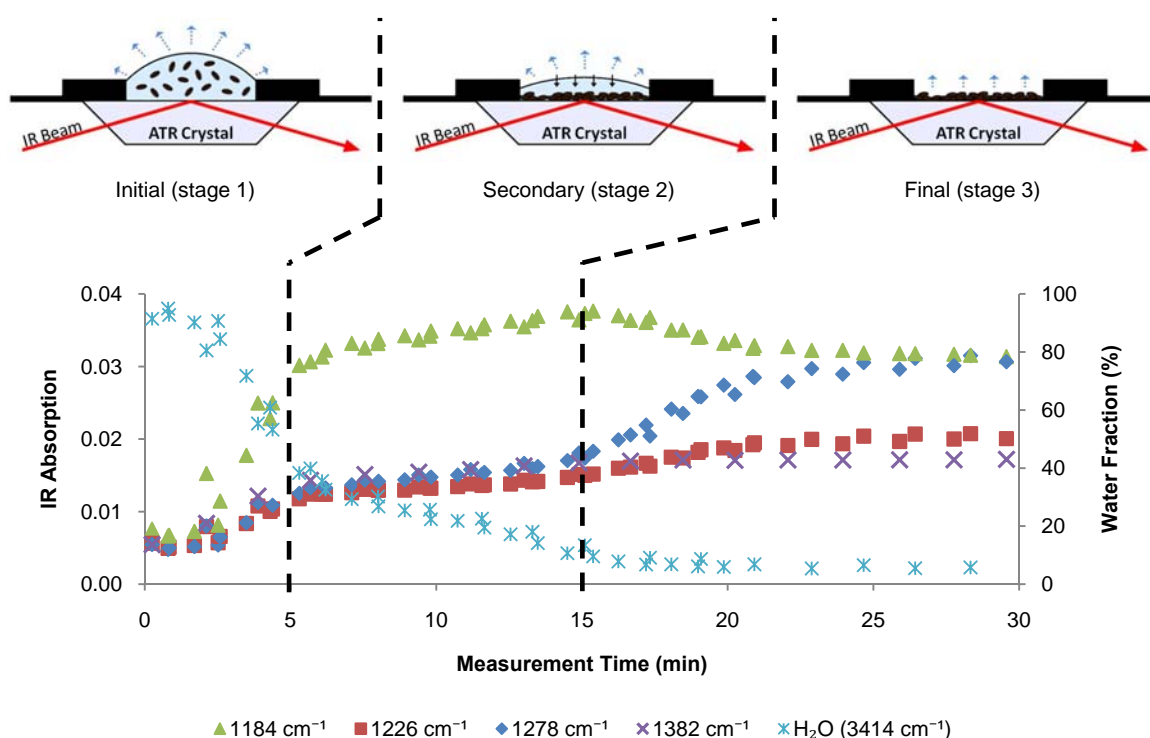


Figure 14. Infrared absorption and water fraction of PHB-containing cells suspended in acidic solution versus measurement time, illustrating three spectral regions: initial (stage 1), where PHB-containing cells are suspended in aqueous solution and free-water begins to evaporate (0-5 min); secondary (stage 2), where free-water continues to evaporate and PHB-containing cells deposit onto ATR window via sedimentation (5-15 min); and final (stage 3), where excess intra-granule water evaporates causing the PHB granules to crystallize (15-30 min)

From the illustrations and the corresponding spectral absorbencies in Figures 13 and 14, it is apparent that water plays a key role in stabilizing the native PHB granules. Free-water, water surrounding the cells and possibly water in the cytosol of the cells, quickly evaporated without changing the crystallinity of the native PHB granules in stage 1 and stage 2 of Figure 14. After some time, the PHB-bound water that resided inside the granules began to evaporate

causing the granules to crystallize in stage 3 of Figure 14. Therefore, the spectral region of interest is the secondary spectrum, as shown with the solid line in Figure 13 and stage 2 of Figure 14, representing to the true, instantaneous crystallinity of PHB.

Similar to pure PHB, the crystallinity of the native PHB granules can be monitored at 1184 cm^{-1} . The wavenumber 1184 cm^{-1} is associated with asymmetric stretching of the C–O–C backbone of PHB, and describes the lateral crystal growth of PHB. As seen in Figure 14, the absorption at 1184 cm^{-1} is much greater than those at 1226 and 1278 cm^{-1} . Additionally, the absorption measured at 1184 cm^{-1} increases during the secondary stage (stage 2), then decreases during the final stage (stage 3). The slight increase seen in stage 2 is attributed to the evaporation of free-water, while the decreasing absorption seen in stage 3 is attributed to the artificial crystallization of PHB induced by the evaporation of intra-granule water. In contrast, the absorbencies observed at 1226 and 1278 cm^{-1} are small, nearly equal to the reference peak 1382 cm^{-1} , and so, more affected by background interference. Moreover, the transition from stage 2 to stage 3 is less apparent at 1226 and 1278 cm^{-1} because the absorbencies at these wavenumbers continually increase throughout the measurement process (stages 1-3). For these reasons, the wavenumber 1184 cm^{-1} is best suited to reflect the actual, *in situ* crystallinity of native PHB granules in microbial cells under varying environmental conditions.

As mentioned, PHB granules are likely stabilized by intra-granule water. The C–H \cdots OH $_2\cdots$ O hydrogen bonds prevent strong dipole-dipole interactions from occurring between the C=O and CH $_3$ groups in PHB (see Figure 4) [6, 23, 29]. Removal of the intra-granule water promotes *in situ* crystallization due to increased C–H \cdots O hydrogen bonding, analogous to the cooling crystallization process in pure PHB [23]. As a result, the molecular mobility of the granules is reduced with excess dehydration, which was observed during the final stage of the ATR-FTIR measurements shown in Figures 13 and 14.

3.6 *In Situ* Crystallinity Measurements via ATR-FTIR Absorption Spectra

The instantaneous crystallinity of native PHB granules can be measured via ATR-FTIR during the secondary stage at wavenumber 1184 cm^{-1} , using similar techniques to that of pure PHB (Sec 3.3-4). Beyond the mechanistic affect of water, vibrational energy absorbed by water generates some degree of background interference in the absorption spectra of the aqueous

solution of cells. Likewise, non-PHB biomass present in the solution causes background interference in the signal. Therefore, the total absorption spectra observed in Figure 13 includes infrared absorbencies from PHB, non-PHB biomass, and water. These components were determined to be additive as seen in the equation [30]:

$$A_{PHB \tilde{\nu}} = A_{total \tilde{\nu}} - (x \cdot A_{biomass \tilde{\nu}} + y \cdot A_{water \tilde{\nu}}) \quad (18)$$

where $A_{m \tilde{\nu}}$ is the infrared absorption of component m at wavenumber $\tilde{\nu}$, and x and y are the weight fractions of the non-PHB biomass and water, respectively. To further investigate the background interference, dried non-PHB biomass from each environmental condition was wetted with varying fractions of water and the resulting spectral data were analyzed. The infrared absorption spectra due to the non-PHB biomass were nearly constant with increasing water fractions, particularly in the range of 30-60% water. Thus, the background interference is assumed constant, so that equation 18 can be reduced to:

$$A_{PHB \tilde{\nu}} = A_{total \tilde{\nu}} - A_{background \tilde{\nu}} \quad (19)$$

where

$$A_{background \tilde{\nu}} = (x \cdot A_{biomass \tilde{\nu}} + y \cdot A_{water \tilde{\nu}}) \cong constant.$$

Applying the same principles as equations 15-17, the instantaneous absorption index (AI_i) at 1184 cm^{-1} and instantaneous crystallinity (X_i) can be calculated from the equations:

$$AI_i = \frac{A_{PHB 1184}}{A_{PHB 1382}} = \frac{A_{total 1184} - A_{background 1184}}{A_{total 1382} - A_{background 1382}} \quad (20)$$

and

$$X_i = m (AI_i) + b \quad (21)$$

where $m = -2.91$ and $b = 3.04$ are the same as shown in Table 3 for the wavenumber 1184 cm^{-1} .

CHAPTER 4

Crystallization of PHB

4.1 Crystallization of Pure PHB

As mentioned (Sec 1.2 and 1.5), the crystallization of PHB is an energetically favorable process, primarily driven by C–H···O hydrogen bonding between the carbonyl (C=O) and methyl (CH₃) groups [17-19]. Referring to Figure 7, the crystallization process of pure PHB from an amorphous melt to a semi-crystalline solid is similar to that of PHBV. First, nucleation occurs when infinitesimally small clusters of amorphous PHB molecules form nuclei [11, 20]. Then, lamellar sheets grow radially outward from nuclei in the form of spherulites [11, 20]. Lastly, secondary crystallization occurs when regions under stress, caused by the impingement of adjacent crystallites or impurities, rearrange into more, energetically favorable structures (Figure 7d) [11, 20].

The primary crystallization process (i.e., nucleation and crystal growth) of pure PHB is well modeled by Avrami's equation for isothermal crystallization [18, 33, 34]:

$$X = 1 - \exp[-k t^n]$$

where X is the crystallinity, t is the crystallization time, n is the Avrami exponent, and k is the crystallization growth rate parameter. Based on the crystallization kinetics of polymers similar to PHB [34, 36], the growth rate parameter may be described by the Arrhenius equation:

$$k^{1/n} = k_o \exp\left[-\frac{\Delta E_a}{R T}\right]$$

where ΔE_a is the crystallization activation energy, R is the gas constant, T is the crystallization temperature, and k_o is a pre-exponential factor independent of the crystallization temperature. Using equations 15-17, the crystallization of pure PHB from a melt at 180°C to a semi-crystalline material at room temperature was monitored with ATR-FTIR at the wavenumber 1184 cm⁻¹ (see Figure 10).

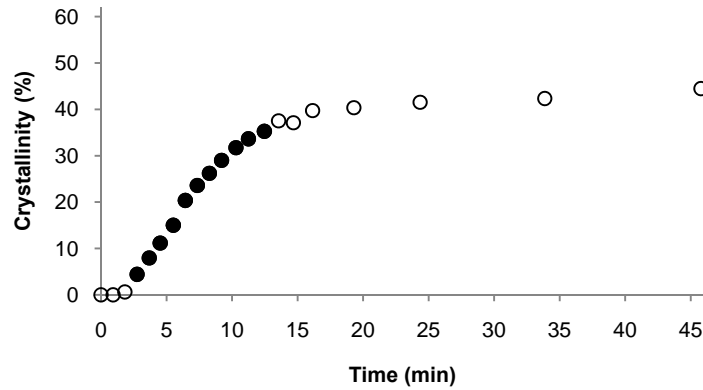


Figure 15. Crystallinity versus time for pure PHB cooled from a melt at 180°C to room temperature in ambient conditions, where ● indicates the primary crystallization region modeled by Avrami's equation

Figure 15 shows a plot of the crystallization of pure PHB, which was melted at 180°C, then, placed on the ATR window at 0 min and allowed to cool at room temperature. Primary crystallization is represented by the solid data points (●), and occurs between 2-15 min. Secondary crystallization occurs after 15 min, indicated by the hollow data points (○). To find the values n and k for the crystallization of the pure PHB sample shown in Figures 10 and 15, Avrami's equation was rewritten as:

$$\log(-\ln(1 - X)) = \log(k) + n \log(t) \quad (22)$$

and $\log(t)$ versus $\log(-\ln(1 - X))$ was plotted in Figure 16 during the primary crystallization stage (2-15 min). The initial data points (0-2 min) are neglected in the Avrami analysis, because the thermal history of the sample may be unstable and is not known. Figure 16 shows a linear trend with slope $n = 1.5010$ and intercept $\log(k) = -1.9264$, where $R^2 = 0.9761$. From the linear correlation, the Avrami exponent (n) and growth rate constant (k) are found:

$$n = 1.5010; k = 0.0118.$$

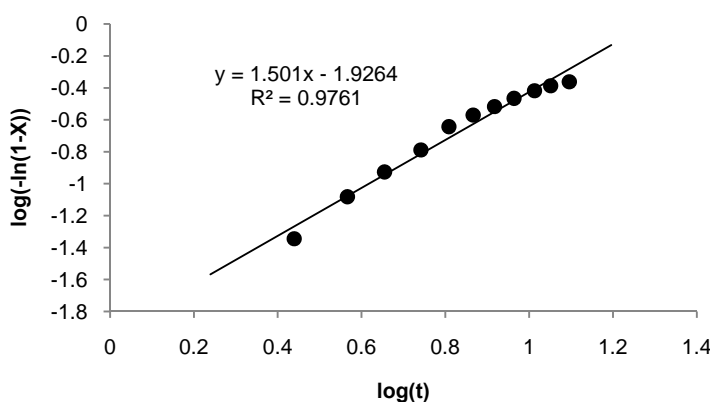


Figure 16. Determination of the crystallization rate constant k and the Avrami exponent n for the crystallization of pure PHB at room temperature during primary crystallization

The parameters n and k describe the geometry of crystal growth and the crystallization growth rate, respectively. When compared to published results from other research groups, these values are within the documented range for the isothermal crystallization of pure PHB [18, 33, 43, 47-49]. The significance of these values depends on the external, mechanical, and thermal properties of the sample (see Sec 4.4 for more information).

4.2 *In Situ* Crystallization of Native PHB Granules

As previously mentioned (Sec 3.5), the PHB-containing cells stored in acidic solution (pH 2) exhibited no biological activity and the PHB granules remained their native state. The mild acidic conditions caused some damage to the cell walls as seen in Figure 12, but did not seem to change the amorphousness, molecular weights, PHB purity, or morphology of the granules.

Figure 17 shows the *in situ* crystallization of native PHB granules suspended in acidic solution (pH 2) measured at room temperature at the wavenumber 1184 cm^{-1} . As noted (Sec 3.5), the instantaneous crystallinity was measured during the secondary stage, after the initial scattering stage and before the final artificial stage. In this figure there are three stages corresponding to the same three stages shown in Figure 14. In the first 5 min after the sample was placed on the ATR window, the fraction of water detected by the infrared beam was very high (60-90%). As a result, data in the initial stage (0-5 min) describing PHB crystallinity was unreliable. After 5-15 min, a significant amount of free-water evaporated and the water fraction

of the signal was reduced to around 30-60%. In this secondary stage (5-15 min) the signal representative of PHB crystallinity stabilized and the instantaneous crystallinity (X_i) could be observed. Lastly, after 15-30 min the PHB crystallinity increased up to 32%, with a corresponding water content of less than 20%. When compared to the crystallization of pure PHB (Figure 15), the final stage (15-30 min) of the native granules followed a similar trend. The instantaneous crystallinity of the native granules averaged over the secondary stage (5-15 min) is $4.89 \pm 1.84\%$. Table 4 contains the slurry properties and crystallinities of three different aqueous solutions of native PHB granules suspended in 0.2 M H_2SO_4 (pH 2).

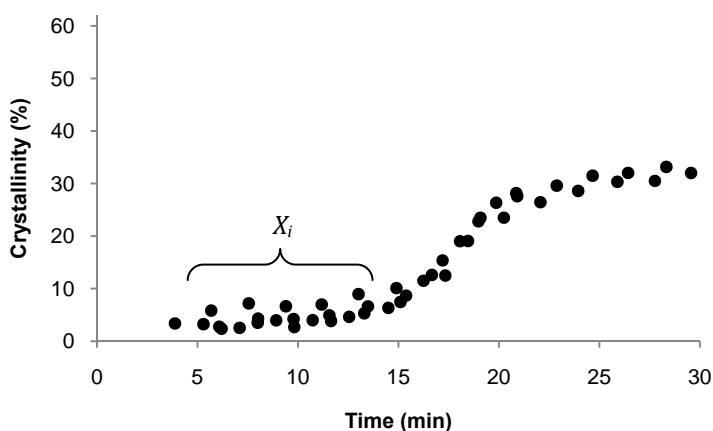


Figure 17. *In situ* crystallinity versus measurement time for native PHB granules in acidic solution (pH 2) at room temperature, illustrating the instantaneous crystallinity at 5-15 mins ($X_i = 4.89 \pm 1.84\%$)

Table 4. Slurry properties of native PHB granules from different aqueous media (0.2 M H_2SO_4)

Slurry	PHB content (%)	Cell mass (g/L)	M_v	$X_i \pm \text{STD}$ (%)
Slurry A	60.0	244	257000	4.89 ± 1.84
Slurry B	66.8	207	186000	6.99 ± 1.41
Slurry C	62.2	165	85000	5.14 ± 2.56

Dehydration of the cells was observed to induce partial crystallization in the native PHB granules without any change in molecular weight or material purity (see Figure 18). Cells (slurry A) freeze-dried for 3 hr exhibited a slow crystallization of PHB, increasing nearly 30% over the first 24 hr after drying. In contrast, cells (slurry A) dehydrated with acetone extraction showed a

much faster crystallization of PHB, nearly twice that of freeze-drying, which is attributed to the simultaneous removal of water and lipids from the granules. Thus, it is concluded that dehydration of the native granules and removal of lipids from the granule membranes induced partial crystallization.

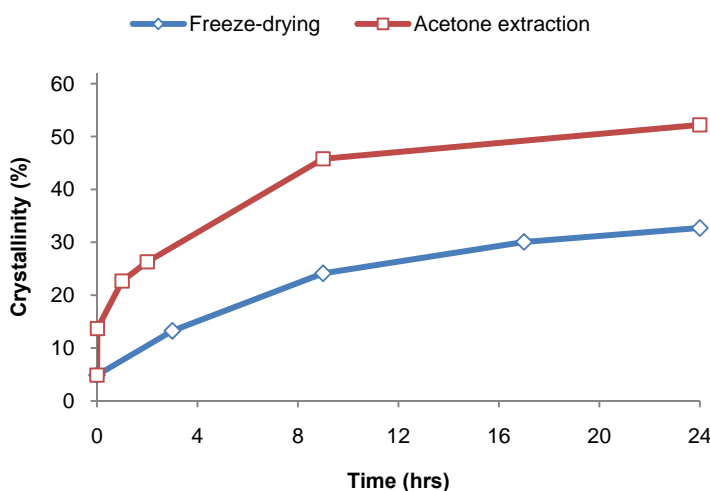


Figure 18. Crystallization of native PHB granules dehydrated by freeze-drying (blue) and acetone extraction (red)

It is widely accepted that PHB granules are fully amorphous *in vivo* having a crystallinity of 0% in a neutral aqueous solution (pH 7) [6, 23]. When partially isolated and/or subjected to varying environmental conditions, however, the PHB granules are believed to undergo varying degrees of crystallization [22, 23, 29]. As expected, the mild acidic solution (pH 2) used to store the PHB-containing cells triggered very minuscule changes in crystallinity (~5%). It seems that the intra-granule water and granule membranes remained largely intact, stabilizing the native PHB granules in a mostly amorphous state. Furthermore, the crystallization that occurred due to excess dehydration during ATR-FTIR measurement and dehydration by freeze-drying did not exceed 35%. Therefore, the remaining granule membranes obviously kept the PHB granules from reaching a fully crystalline state (~60%). When dehydrated with acetone, on the other hand, the native granules became highly crystalline (~52%) after 24 hr, further suggesting that the lipids dissolved in acetone (~20 wt%) stabilized the native granules in an amorphous state.

4.3 Modeling the *In Situ* Crystallization of PHB Granules in Different Environments

Similar to the crystallization of pure PHB, the *in situ* crystallization of PHB granules in different environmental conditions (i.e., heat and pH) is modeled by Avrami's equation:

$$X_i = 1 - \exp[-k t^n] \quad (23)$$

where X_i is the instantaneous crystallinity of the granules, t is the exposure time of the granules in a particular environment, n is the Avrami exponent, and k is the crystallization growth rate parameter. Through empirical relations of crystallinity with exposure time, temperature and pH, the Avrami exponents (n) and growth rate parameters (k) may be evaluated and described according to the granule environment.

4.3.1 Heated PHB Granules

PHB granules (slurry A) heated and maintained at high temperature (80-140°C) in acidic solution (pH 2) showed an increase in PHB purity and decrease in molecular weight with increasing temperature and exposure time. Figure 19a is a representative plot of the molecular weight degradation and PHB content increase of the native PHB granules heated at 120°C over 4 hr. Figure 19b is a representative TEM picture of the heated PHB granules at 120°C for 1 hr. After 1 hr at 120°C, the heated granules showed moderate aggregation, a decrease in relative molecular weight of about 50%, and an increase in PHB purity and corresponding protein release of about 15%.

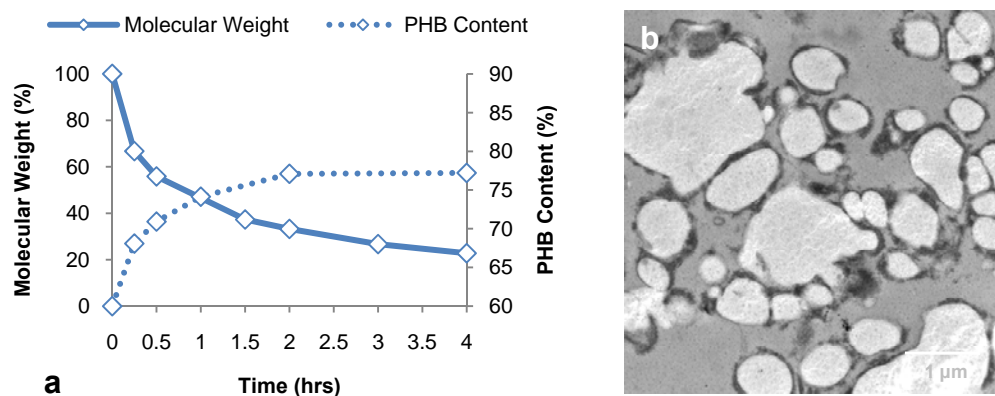


Figure 19. PHB granules heated at 120°C in acidic solution (pH 2): (a) relative molecular weight and PHB content versus exposure time; (b) TEM image of granules at 120°C for 1 hr

Figure 20 shows representative plots of the ATR-FTIR measurements of heated PHB granules (slurry A) in acidic solution (pH 2) at 120°C for 1 hr. In contrast to Figure 17, the plot of the heated granules (Figure 20b) does not contain three temporal stages. Although there was an initial scattered stage due to high water content (0-5 min), there did not seem to be separate secondary and final stages, as observed in the native granules. Instead, the heated granules immediately exhibited a stable crystallinity due to the harsh treatment conditions. The absence of a final artificial crystallization stage suggests that high temperatures may cause the PHB molecules to rearrange with other biological components, including lipids and proteins, and no longer be stabilized by intra-granule water. Therefore, excess dehydration of the cells did not induce any artificial crystallization in the heated granules. The instantaneous crystallinity of the heated granules averaged over the stable region (15-60 min) is $22.52 \pm 2.43\%$.

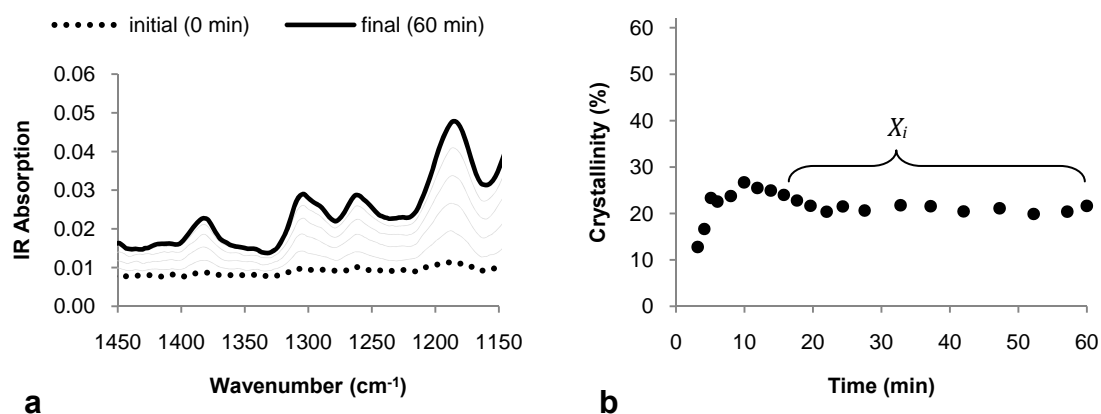


Figure 20. ATR-FTIR measurements for heated PHB granules (120°C, 1 hr) in acidic solution (pH 2): (a) time development of the infrared absorption spectra; (b) *in situ* crystallinity versus measurement time, illustrating the instantaneous crystallinity at 15-60 mins ($X_i = 22.52 \pm 2.43\%$)

Figure 21 shows the *in situ* crystallization of PHB granules (slurry A) heated at 80-140°C in acidic solution (pH 2) over 4 hr. Applying Avrami's equation to the data plotted in Figure 21, similar to that of pure PHB (22), the crystallinity becomes a linear function of exposure time at constant temperature:

$$\log(-\ln(1 - X_i)) = \log(k) + n \log(t) \quad (24)$$

where X_i is the instantaneous crystallinity and t is the exposure time of the granules at temperature T .

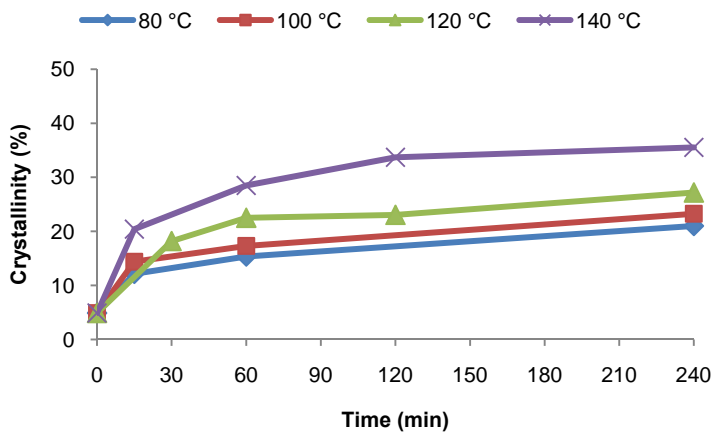


Figure 21. Crystallization of PHB granules heated at 80-140°C over 4 hrs

Figure 22 shows a log-log plot illustrating the linear correlations. Table 5 contains values of the Avrami exponents (n) and growth rate parameters (k) for temperatures 80-140°C. From observation of the values, it is apparent that the Avrami exponent remains constant with temperature (see Table 5):

$$n = 0.2140 \pm 0.0234.$$

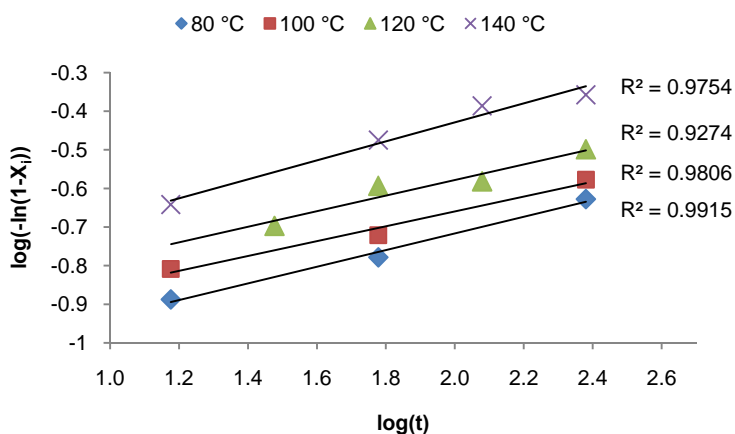


Figure 22. Log-log plot illustrating the linearity of *in situ* crystallization versus time of heated PHB granules

Further analysis shows that the crystallization growth rate parameter is function of temperature following the Arrhenius equation (see Figure 23):

$$k^{1/n} = k_o \exp \left[-\frac{\Delta E_a}{R T} \right]$$

where T is the temperature in Kelvin and R is the gas constant (8.314 J/K·mol). Rewriting the equation:

$$\frac{1}{n} \ln(k) = \ln(k_o) - \frac{\Delta E_a}{R} \left(\frac{1}{T} \right) \quad (25)$$

and plotting $(1/n) \ln(k)$ versus $1/T$, the pre-exponential factor and activation energy are found from the linear correlation shown in Figure 23 to be $k_o = 78.73 \text{ min}^{-1}$ and $\Delta E_a = 48.82 \text{ kJ/mol}$, respectively. When compared to the activation energy of polypropylene (163 kJ/mol), the activation energy determined for the heated PHB granules (48.82 kJ/mol) is lower, but of the same magnitude [34]. This relationship is very well correlated to the crystallization data from the heated granules ($R^2 = 0.9903$) and the range of the growth rate parameter is $k = 0.0725$ - 0.1215 for 80 - 140°C (see Table 5).

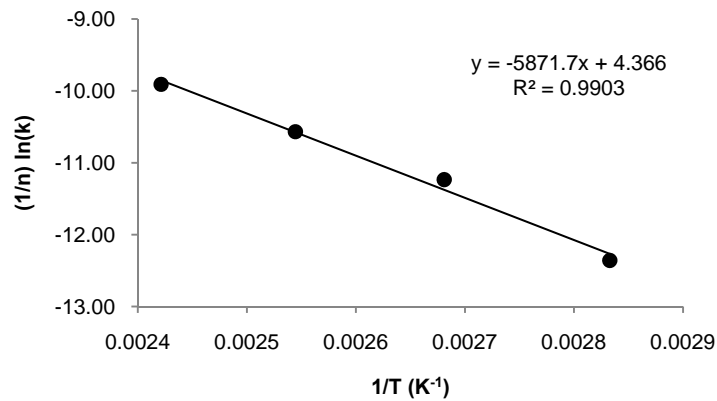


Figure 23. Crystallization growth rate parameter k as a function of temperature for heated PHB granules

Table 5. Crystallization parameters of the heated PHB granules (slurry A) from Avrami analysis

Temperature (°C)	n	$k(\text{min}^{-n})$	R^2	$(1/n) \ln(k)$	$1/T$
80	0.2159	0.0711	0.9915	-12.36	0.0028
100	0.1922	0.0904	0.9806	-11.23	0.0027
120	0.2018	0.1042	0.9274	-10.57	0.0025
140	0.2459	0.1200	0.9754	-9.91	0.0024
AVG	0.2140	---	---	---	---
STD	0.0234	---	---	---	---

4.3.2 Alkaline PHB Granules

Similar to the heated granules, PHB granules (slurry B) with increasing pH at room temperature showed an increase in PHB purity and decrease in molecular weight. Figure 24a is a representative plot of the molecule degradation and PHB content increase of the PHB granules in alkaline solution (pH 12) over 4 hr. Figure 24b is a representative TEM picture of the alkaline PHB granules at pH 12. After 1 hr of treatment at pH 12, the alkaline granules showed very little to no aggregation, a decrease in molecular weight of about 70%, and an increase in PHB purity and corresponding protein release of about 15%.

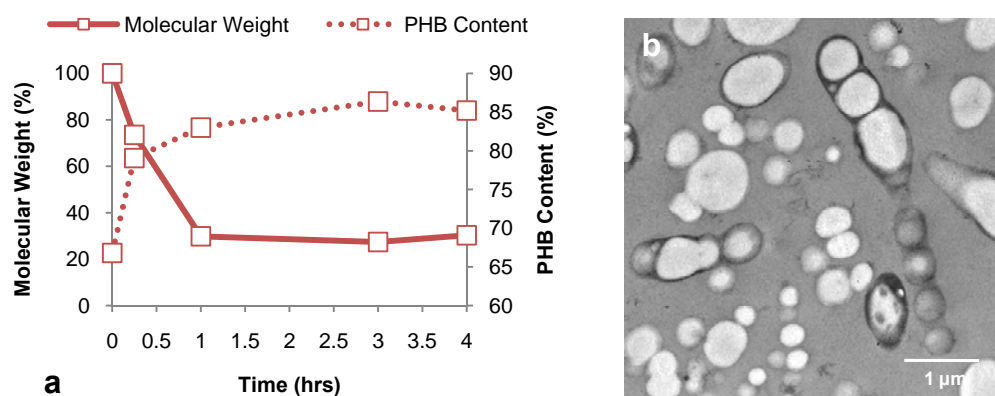


Figure 24. PHB granules in alkaline solution (pH 12) at room temperature: (a) relative molecular weight and PHB content versus exposure time; (b) TEM image of granules at pH 12 for 1 hr

Figure 25 shows representative plots of the ATR-FTIR measurements of the alkaline granules (slurry B) at pH 12 for 1 hr. Similar to Figure 17, the plot of the alkaline granules (Figure 25b) shows three temporal stages: an initial scattered stage due to high water content (0-3 min), a stable stage representing the true, instantaneous crystallinity of the granules (3-5 min), and a final stage of artificial crystallization caused by excess dehydration of the sample (5-12 min). Unlike the native granules, however, the alkaline granules (pH 12) were observed in a highly crystalline state prior to excess dehydration and showed a rapid increase in crystallinity after 5 min of measurement. Therefore, it may be concluded that increasing the pH of the native granules may cause the granules to undergo rapid crystallization due to the dissolution of lipids and proteins from the granule membrane. The instantaneous crystallinity of the alkaline granules averaged over the stable region (3-5 min) is $40.59 \pm 1.92\%$.

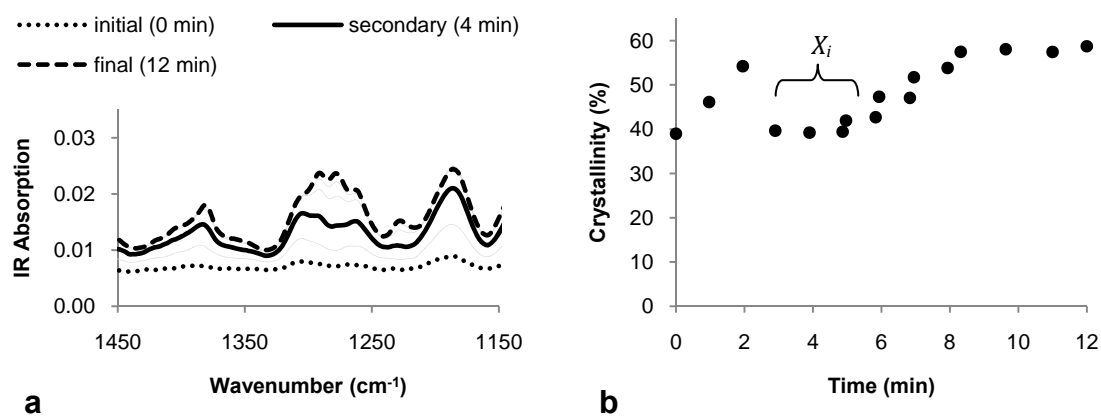


Figure 25. ATR-FTIR measurements for alkaline PHB granules (pH 12, 1 hr): (a) time development of the infrared absorption spectra; (b) *in situ* crystallinity versus measurement time, illustrating the instantaneous crystallinity at 3-5 mins ($X_i = 40.59 \pm 1.92\%$)

Figure 26 shows the *in situ* crystallization of PHB granules (slurry B) in aqueous solutions of varying pH over 4 hr. As seen in the plot, the crystallinity does not seem to increase significantly with exposure time. Therefore, the crystallinity was assumed to be independent of time, so that Avrami's equation (23) can be reduced as follows:

$$\log(-\ln(1 - X_i)) = \log(k) \quad (26)$$

where X_i is the average crystallinity of the granules at a particular pH, and $n \log(t)$ drops out, so that the Avrami exponent can be assumed null:

$$n \rightarrow 0.$$

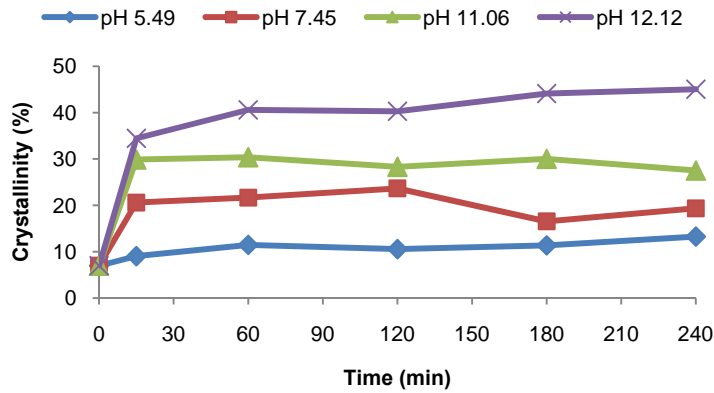


Figure 26. Crystallization of PHB granules with varying pH over 4 hrs

Then the right hand side of equation 26 can be plotted as a function of pOH (see Figure 27), where:

$$\text{pOH} = -\log [\text{OH}^-] \quad (27)$$

and $\text{pH} + \text{pOH} = 14$. From the log plot in Figure 27 it is apparent that the crystallinity of the PHB granules is linearly correlated to the pOH of the solution (see Table 6):

$$\log(-\ln(1 - X_i)) = \alpha (\text{pOH}) + \beta \quad (28)$$

where the constants $\alpha = -0.0891$ and $\beta = -0.1219$. Finally, combining equations 26, 27, and 28 yields an expression for the crystallization growth rate parameter:

$$k = (10^\beta)[\text{OH}^-]^\alpha \quad (29)$$

where $[\text{OH}^-]$ is the concentration of hydroxide ions in the solution. No temperature dependence appears in this equation (29) because the pH of the granules was adjusted at constant room temperature. This empirical relationship is well correlated to the crystallization data from the PHB granules with increasing pH ($R^2 = 0.9727$) and the range of the growth rate parameter is $k = 0.0428\text{-}0.7553$ for pH 0-14 (see Table 6).

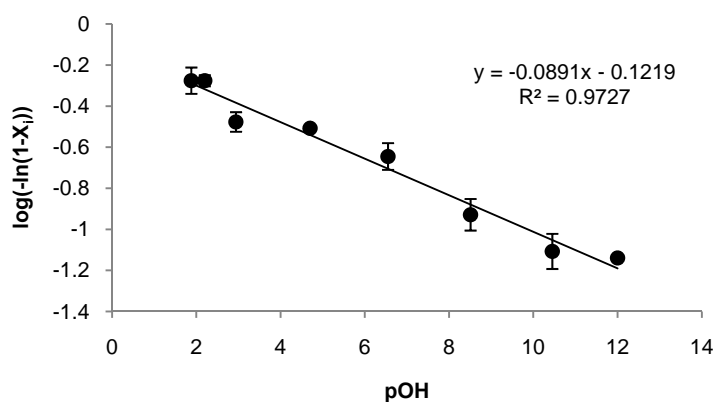


Figure 27. Log plot illustrating the linearity of *in situ* crystallization versus pOH of alkaline PHB granules

Table 6. Crystallization parameters of the PHB granules (slurry B) with increasing pH from Avrami analysis

pH	$X_i \pm \text{STD} (\%)$	$\log(-\ln(1 - X_i))$	n	$k (\text{min}^{-n})$
2.00	6.99 \pm 1.41	-1.14	0.00	0.0645
3.55	7.61 \pm 1.36	-1.11	↓	0.0886
5.49	11.24 \pm 1.97	-0.93		0.1319
7.45	20.37 \pm 2.65	-0.65		0.1972
9.30	26.70 \pm 0.52	-0.51		0.2881
11.06	28.43 \pm 2.65	-0.48		0.4133
11.80	41.14 \pm 1.96	-0.28		0.4811
12.12	41.25 \pm 4.63	-0.28		0.5137

4.4 Interpretation Avrami Exponents and Growth Rate Parameters

Table 7 contains the equations and empirical constants determined from the Avrami analyses for the crystallization of pure PHB, the heated PHB granules in acidic solution (pH 2), and the alkaline PHB granules at room temperature. As previously shown (Sec 4.1 and 4.3.1-2), Avrami's equation can be used to describe the crystallization of pure PHB, as well as, the *in situ* crystallization of native PHB granules in different environmental conditions. Differences in the Avrami exponents (n) and growth rate parameters (k) for each condition provide the insight necessary to understand the different crystallization processes. Figure 28 illustrates the theoretical crystallization phenomenon for each of the cases described in Table 7.

Table 7. Crystallization models of pure PHB and PHB granules in varying environments by Avrami analysis

	Pure PHB	Heated PHB Granules	Alkaline PHB Granules
<i>Crystallinity</i>	$X = 1 - \exp[-k t^n]$	$X_i = 1 - \exp[-k t^n]$	$X_i = 1 - \exp[-k t^n]$
<i>Growth Rate Parameter</i>	$k^{1/n} = k_o \exp\left[-\frac{\Delta E_a}{R T}\right]$	$k^{1/n} = k_o \exp\left[-\frac{\Delta E_a}{R T}\right]$ $k_o = 78.73 \text{ min}^{-1}; \Delta E_a = 48.82 \text{ kJ/mol}$	$k = (10^\beta)[\text{OH}^-]^\alpha$ $\alpha = -0.0891; \beta = -0.1219$
<i>n</i>	1.5010	0.2140	0
<i>k (min⁻ⁿ)</i>	0.0118	0.0725 - 0.1215 ^a	0.0428 - 0.7553 ^b
<i>R²</i>	0.9761	0.9903	0.9727

^a Range of *k* for temperatures 80-140°C

^b Range of *k* for pH 0-14

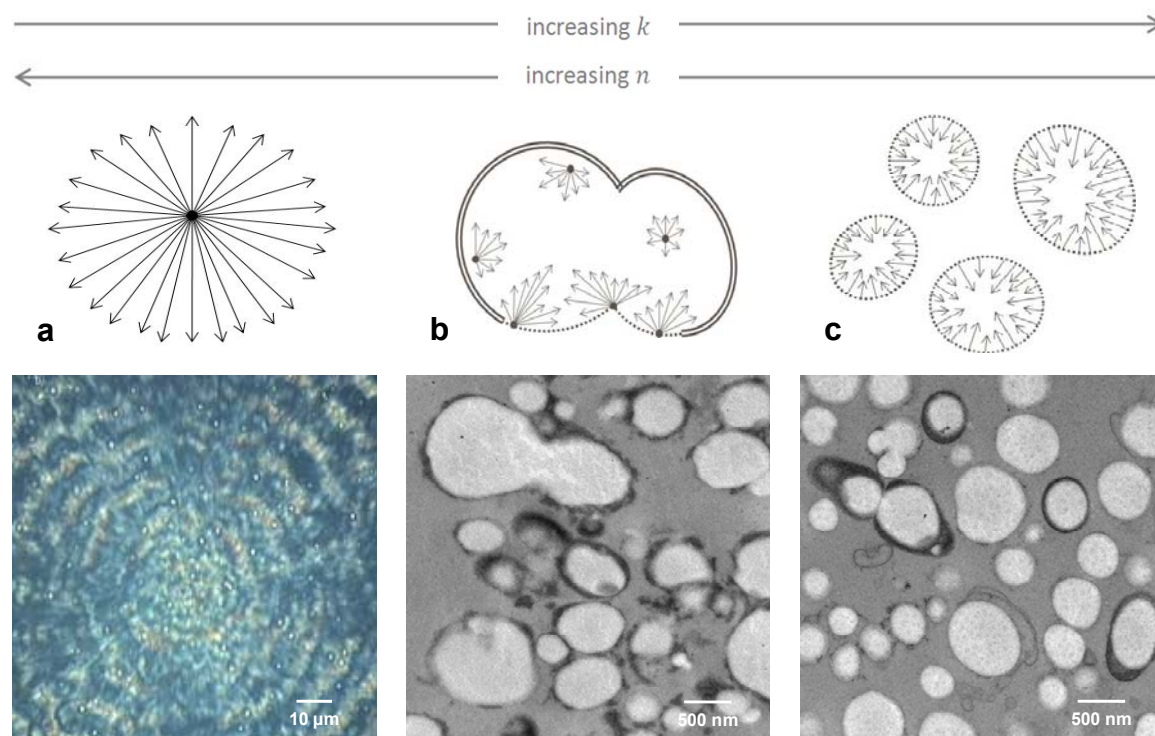


Figure 28. Illustrations of PHB crystallization: (a) *pure PHB*, spherulitic crystal growth from infinitesimal point source nuclei; (b) *heated PHB granules*, moderate granule aggregation and random crystal growth where intra-granule water and membranes are displaced; (c) *alkaline PHB granules*, instant crystal growth inward from granule surfaces lacking membranes

To help visualize the crystallization processes, it is useful to first introduce the following size parameter for crystal growth:

$$w = \frac{r_n}{r_s} \quad (30)$$

where the average radii of the nuclei and corresponding spherulites are r_n and r_s , respectively. Simply put, the size parameter will approach zero ($w \rightarrow 0$) for large spherulites grown from tiny nuclei, and unity ($w \rightarrow 1$) when nucleation occurs instantaneously without subsequent spherulitic crystal growth. That is, the smallest possible crystallite that can exist is, in fact, a nucleus [20].

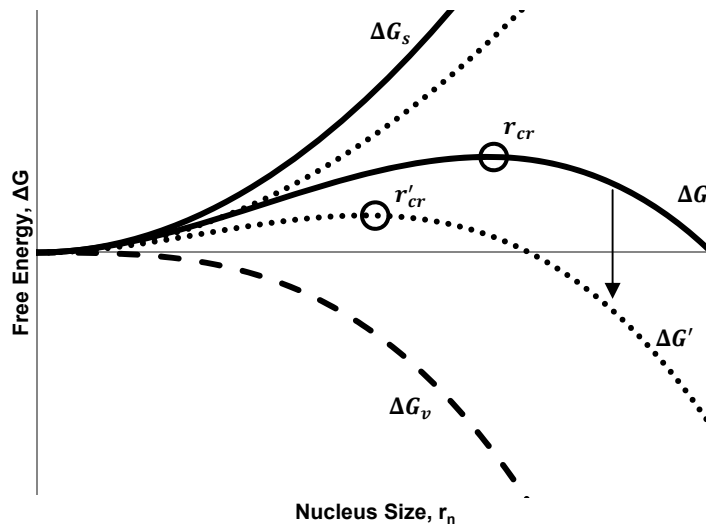


Figure 29. Free energy versus cluster radius for homogeneous (solid line) and heterogeneous (dotted line) nucleation, where ΔG is the total Gibbs free energy, ΔG_s is the surface energy component, ΔG_v is the volume energy component (dashed line), r_{cr} is the critical radius (primed values indicate parameters associated with a lowered free energy barrier due to heterogeneous nucleation) [20, 32]

To explain the driving forces behind nucleation, it is necessary to introduce the Gibbs free energy requirement (see Figure 29) for the formation of a nucleus (first term) and the creation of new phase boundaries associated with nucleation (second term) [20, 32]:

$$\Delta G = aL^2\sigma + bL^3\Delta G_v \quad (31)$$

where a and b are shape factors dependent on the characteristic crystal length L , σ is the energy per unit area (i.e., surface energy), and ΔG_v is the energy per unit volume. Assuming spherical nuclei of characteristic radius r , the shape factors become $a = \pi$ and $b = \pi/6$ so that equation 31 becomes [20]:

$$\Delta G = 4\pi r^2 \sigma + \frac{4}{3}\pi r^3 \Delta G_v. \quad (32)$$

Then, minimizing the equation ($d\Delta G/dr = 0$), the critical nucleus size (critical radius) required to overcome the free energy barrier for nucleation is [20, 32]:

$$r_{cr} = -\frac{2\sigma}{\Delta G_v}. \quad (33)$$

Upon inspection of this term (see Figure 29), it is apparent that surface energy ($\sigma \propto \Delta G_s$) dominates when the average nuclei radius is less than the critical radius ($r_n < r_{cr}$), and volumetric energy (ΔG_v) dominates when the average nuclei radius is greater than the critical radius ($r_n > r_{cr}$) [20, 32]. That is, small nuclei ($r_n < r_{cr}$) are thermodynamically unfavorable and can only occur on surfaces where the free energy barrier has been lowered by external factors, such as granule impurities or external forces (i.e., heterogeneous nucleation, Figure 29 dotted line). Large nuclei ($r_n > r_{cr}$), on the other hand, are thermodynamically favorable so that polymers tend to aggregate into small clusters and grow from a finite volume (i.e., homogeneous nucleation, Figure 29 solid line).

As seen in Figure 28a, the nuclei in pure PHB can be considered point-sources of infinite crystal growth, where spherulites grow radially outward. Therefore, the average nuclei radius becomes much smaller than the average spherulite radius with time ($r_n \ll r_s$), so that $w \rightarrow 0$. Because pure PHB is a neat homopolymer, the nucleation sites are likely dominated by volumetric energy ($r_n > r_{cr}$), assuming no impurities or external forces are present during crystallization [20]. This assumption ($r_n > r_{cr}$) is inherent of point-source, or homogeneous, nucleation [20, 32].

In Figure 28b, the heated PHB granules are shown to crystallize at random locations throughout each granule. Aggregation of the heated granules is assumed to occur only at regions where PHB is amorphous, and intermolecular entanglement can easily take place. Moreover, intra-granule water is assumed to be displaced from the heated granules and no longer acts as a plasticizer of PHB (refer to Sec 4.3.1, Figure 20). Therefore, nucleation in the

heated granules is most likely driven by thermal energy at surfaces where the granule membranes have ruptured or intra-granule water has been displaced. Comparing the optical image descriptive of PHB (Figure 28a) with the TEM image of the heated granules (Figure 28b) it is apparent that the heated granules ($< 2 \mu\text{m}$) have much less available material (PHB per granule) to crystallize than pure PHB ($> 10 \mu\text{m}$). As a result, the final size parameter (ratio of nuclei to spherulite radius) of the heated granules is larger than that of pure PHB, so that $0 < w < 1$. Considering the presence of impurities (i.e., non-PHB biomass and water), the average nuclei radius of the heated granules is most likely less than the critical radius ($r_n < r_{cr}$), corresponding to surface dominated, or heterogeneous, nucleation.

In Figure 28c, the alkaline PHB granules are shown to crystallize from the granule surfaces, inward. Physically, this surface-crystallization phenomenon makes sense because there was almost no aggregation of the alkaline granules. That is, the amorphous regions of the alkaline granules must be in the interior, stabilized by intra-granule water (refer to Sec 4.3.2, Figure 25), and therefore unable to aggregate. Comparing the TEM images of the PHB granules (Figure 28b and 28c) it is obvious that the alkaline granules ($< 0.5 \mu\text{m}$) have less available material (PHB per granule) for crystal growth than the heated granules ($< 2 \mu\text{m}$). Thus, the PHB crystallites in the alkaline granules are geometrically restricted and may not grow beyond the initial nucleus size ($r_s \approx r_n$), so that $w \rightarrow 1$. This suggests that crystallization of the alkaline granules is virtually instantaneous – in agreement with the observation that $n \rightarrow 0$ (Sec 4.3.2). Again, considering the presence of non-PHB biomass and water, the average nuclei radius of the alkaline granules is likely less than the critical radius ($r_n < r_{cr}$), corresponding to surface dominated, heterogeneous nucleation.

From a physical standpoint, the Avrami exponent (n) is a measure of the geometric constraints associated with isothermal crystallization and may be related to the theoretical size ratio (w) discussed above. More precisely, the nature of nucleation (i.e., number and size of nucleation points) and the type of crystal growth (i.e., geometry of spherulites) are described by the Avrami exponent. A large Avrami exponent ($n > 1$) may signify relatively large spherulitic growth ($w \rightarrow 0$) and favorable, point-source (homogeneous) nucleation ($r_n > r_{cr}$), as seen in pure PHB where $n = 1.5010$. A small Avrami exponent ($n < 1$) most likely represents smaller spherulitic crystal growth ($0 \leq w < 1$) and unfavorable, surface-source nucleation ($r_n < r_{cr}$), as seen in the heated granules where $n = 0.2140$ and the alkaline granules where $n = 0$. This

surface nucleation phenomenon probably occurs at interfacial surfaces created by the removal of non-PHB biomass and water, lowering the free energy barrier, allowing a greater number of smaller nuclei to crystallize. As the Avrami exponent approaches zero ($n \rightarrow 0$), the size of spherulites may be restricted by material availability (PHB per granule) and unable to grow beyond size of the nuclei ($w \rightarrow 1$), as seen in the alkaline granules where $n = 0$. This behavior ($n \rightarrow 0$) is indicative of nearly instantaneous (time independent) crystal growth, where crystalline regions are composed of several tiny crystallites the size of individual nuclei.

A more straightforward description of crystallization is the growth rate parameter (k), which is a measure of the kinetics associated with the average nucleation and spherulitic growth of a single crystal. That is, the larger a spherulite can grow, the lower the growth rate parameter because it takes more time to fully crystallize than a smaller spherulite. As seen in Tables 5, 6 and 7, the growth rate parameter is smallest for pure PHB where $k = 0.0118$ and increases with increasing temperature ($k \rightarrow 0.1215$) and increasing pH ($k \rightarrow 0.7553$). This suggests that a single spherulitic crystal of pure PHB ($> 10 \mu\text{m}$) takes significantly longer time to fully crystallize than the smaller random crystals of the heated granules ($< 2 \mu\text{m}$) and alkaline granules ($< 0.5 \mu\text{m}$) respectively. Molecular weight may also affect the growth rate parameter because shorter polymer chains should take less time to crystallize than longer polymer chains.

Figure 28 shows the general trends of increasing n and k with respect to the PHB crystallization events described for the three cases shown in Table 7. In summary, the empirical values of n and k increase and decrease respectively, with the amount of available material (i.e., PHB per crystal/granule) for the nucleation and crystal growth. Pure PHB crystallizes into large spherulitic structures from homogeneous nuclei ($n = 1.5010$) at a slow growth rate ($k = 0.0118$). Heated PHB granules crystallize into partial spherulitic structures from heterogeneous nuclei ($n = 0.2140$) at moderate growth rates ($k = 0.0725$ - 0.1215). And, alkaline PHB granules crystallize instantaneously from heterogeneous nuclei at granule surfaces ($n = 0$) at fast growth rates ($k = 0.0428$ - 0.7553).

CHAPTER 5

BEHAVIOR OF PHB GRANULES IN MILD CONDITIONS

Mild external factors, such as centrifugation, ultrasonication, and surfactant, were shown to trigger little to no *in situ* crystallization of the native PHB granules. Although the mild conditions did not significantly change the granule crystallinity, molecular weight or PHB purity, the highly amorphous granules showed varying degrees of aggregation.

5.1 Centrifuged PHB Granules

Centrifugation (1250-10000 g) of the native PHB granules (slurry A) for 1 hr showed a slight increase in PHB crystallinity (~10%) with no change in molecular weight or PHB purity. This result agrees with the assumption that centrifugation may induce partial crystallization due to the close packing and subsequent inactivation of the PHB granules [24, 29]. The slight increase in crystallinity was nearly identical for centrifugal forces of 1250-10000 g (see Figure 30), suggesting that centrifugal force has very little influence on PHB crystallinity. Figure 31 shows SEM images of freeze-dried cells before and after centrifugation. As seen in the second image (Figure 31b), the granules showed little aggregated upon centrifugation because there appears to be stretched tendrils of polymeric material between adjacent clusters of cells, further proving that the centrifuged PHB granules were predominately amorphous.

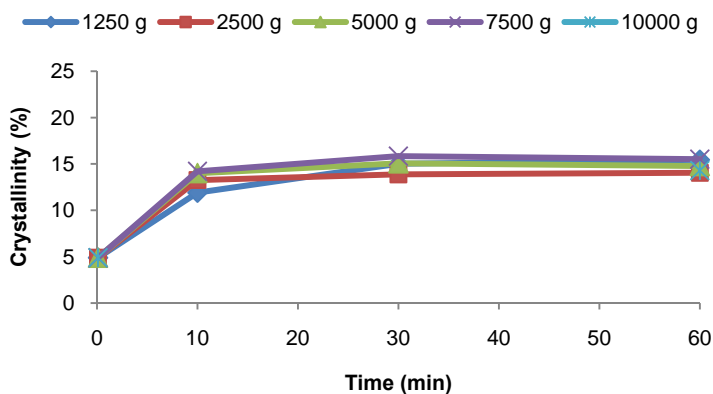


Figure 30. Crystallization of PHB granules centrifuged at 1250-10000 g over 1 hr

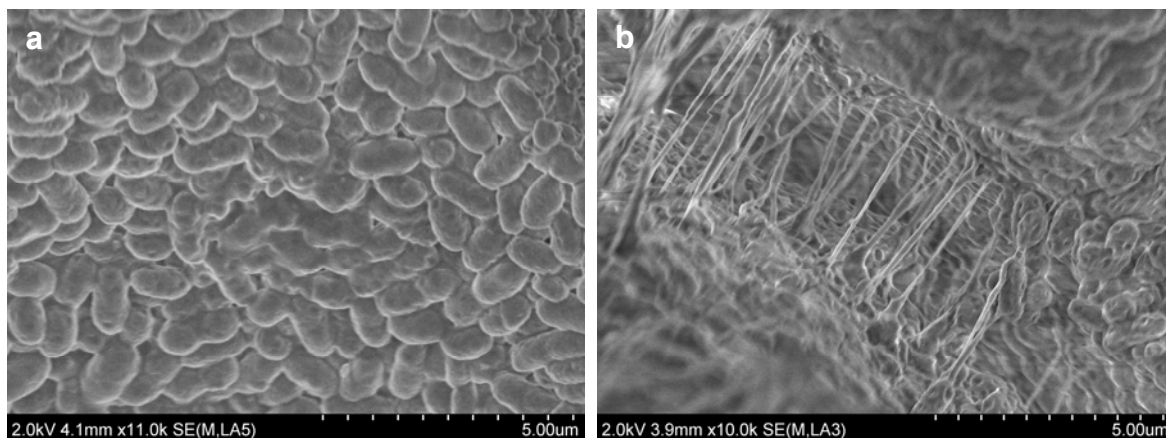


Figure 31. SEM images of cells: (a) before centrifugation; (b) after centrifugation at 5000 g for 30 min

5.2 Ultrasonicated PHB Granules

Ultrasonication at 22.5 kHz (0-300 J/mL) of the native PHB granules (slurry C) induced little crystallization and molecule degradation with a small increase in material purity. As seen in Figure 32a, the relative molecular weight of the ultrasonicated granules was reduced about 15%, while the corresponding increase in PHB crystallinity was almost 10% at 300 J/mL. The PHB content of the ultrasonicated granules at 300 J/mL increased only 5%. Figure 32b shows a TEM image of ultrasonicated granules with an energy input of 4.5 kJ/mL. The moderate granule aggregation observed here, agrees with the conclusion that little *in situ* crystallization is induced by ultrasonication.

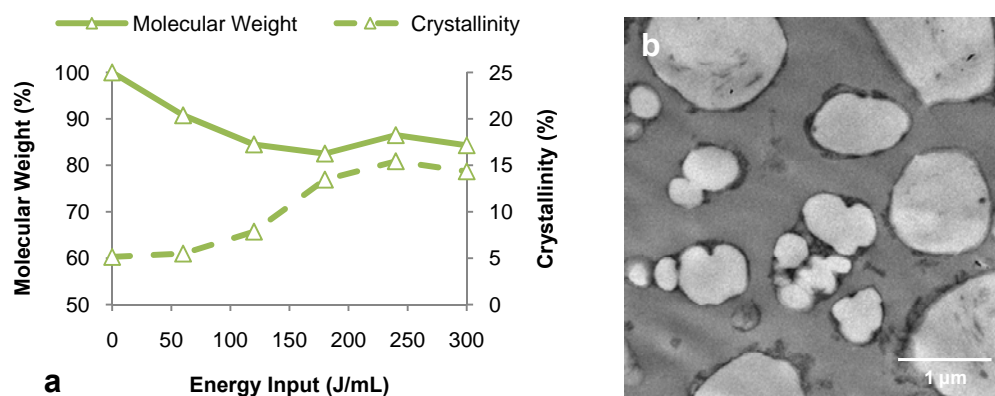


Figure 32. Ultrasonicated PHB granules at 22.5 kHz: (a) relative molecular weight and *in situ* crystallinity versus energy input; (b) TEM image of native granules ultrasonicated at 4.5 kJ/mL

5.3 PHB Granules with Surfactant

In further investigation, native PHB granules (slurry B) treated with the surfactant sodium dodecyl sulfate (SDS) remained unchanged in terms of material purity and molecular weight. Based on ATR-FTIR measurements at low concentrations of SDS (0-12.5 g/L), the native granules showed very little to no increase in crystallinity. At high concentrations of SDS (25-50 g/L), however, the ATR-FTIR measurements were unreliable due to spectral interference from infrared absorptions characteristic of SDS (see Figure 33). Therefore, TEM pictures of PHB granules treated with 50 g/L SDS were used to determine the apparent crystallinity. Figure 34 shows that PHB granules treated with SDS experienced extensive granule aggregation – supporting the assumption that PHB granules treated with surfactant remained amorphous. It seems that the surfactant may stabilize the amorphous granules in a similar manner to that of the lipids in the native granule membranes.

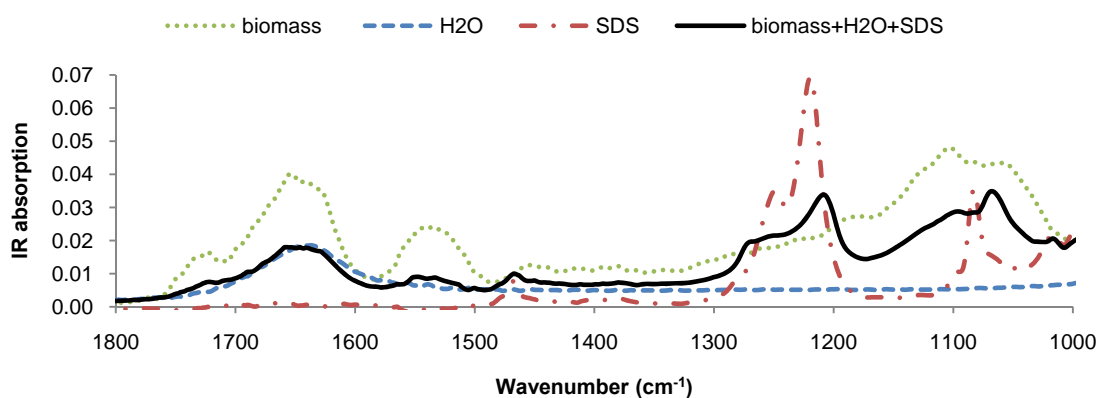


Figure 33. ATR-FTIR spectral background interference of non-PHB biomass, water, and 50 g/L SDS

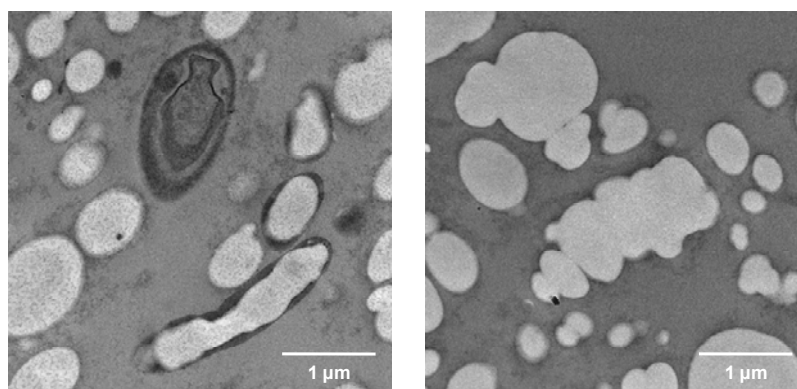


Figure 34. TEM images of PHB granules treated with 50 g/L SDS

CHAPTER 6

PROPERTIES OF PHB GRANULES OF DIFFERENT CRYSTALLINITY

The *in situ* crystallization of PHB was shown to toughen the granules against granule aggregation and molecule degradation. Changes in the granule properties, such as granule morphology and molecular weight, are assumed to occur in regions where PHB is amorphous, and can easily come in contact with other molecules. As previously observed (Sec 4.3.1-2 and CHAPTER 5), varying environmental conditions induce varying degrees of granule aggregation and molecule degradation, which are determined to depend on degree of crystallinity.

6.1 Granule Morphology

Table 8 shows the *in situ* crystallinity, state of the granule membrane (i.e., intact or ruptured) and extent of granule aggregation for the native PHB granules in different environmental conditions. Corresponding to Table 8 are TEM pictures collected for the different environmental conditions, shown in Figure 35, and SEM pictures in Figure 31.

Table 8. Crystallinity and state of granule membrane versus granule morphology (i.e., aggregation)

Sample	Crystallinity (%)	Membrane	Aggregation	Morphology
PHB granules <i>in vivo</i> (pH 7)	0	Native	None	Fig 35a
Native granules (pH 2)	4.89-6.99	Intact	None	Fig 35b
Granules w/ surfactant (50 g/L SDS)	(6.99) ^a	Ruptured	Extensive	Fig 35f
Centrifuged granules (10000 g, 1 hr)	14.29	Partially Intact	Little	Fig 31b
Ultrasonicated granules (300 J/mL)	14.35	Ruptured	Moderate	Fig 35e
Heated granules (120°C, 1 hr)	22.52	Ruptured	Moderate	Fig 35d
Dehydrated granules (24 hrs)	32.71	Intact	None	Fig 31a
Alkaline granules (pH 12, 1 hr)	40.59	Ruptured	Little	Fig 35c

^a Although *in situ* crystallinity of PHB granules w/ surfactant cannot be determined with ATR-FTIR, it is reasonable to assume the PHB granules remain amorphous in SDS (Sec 5.3)

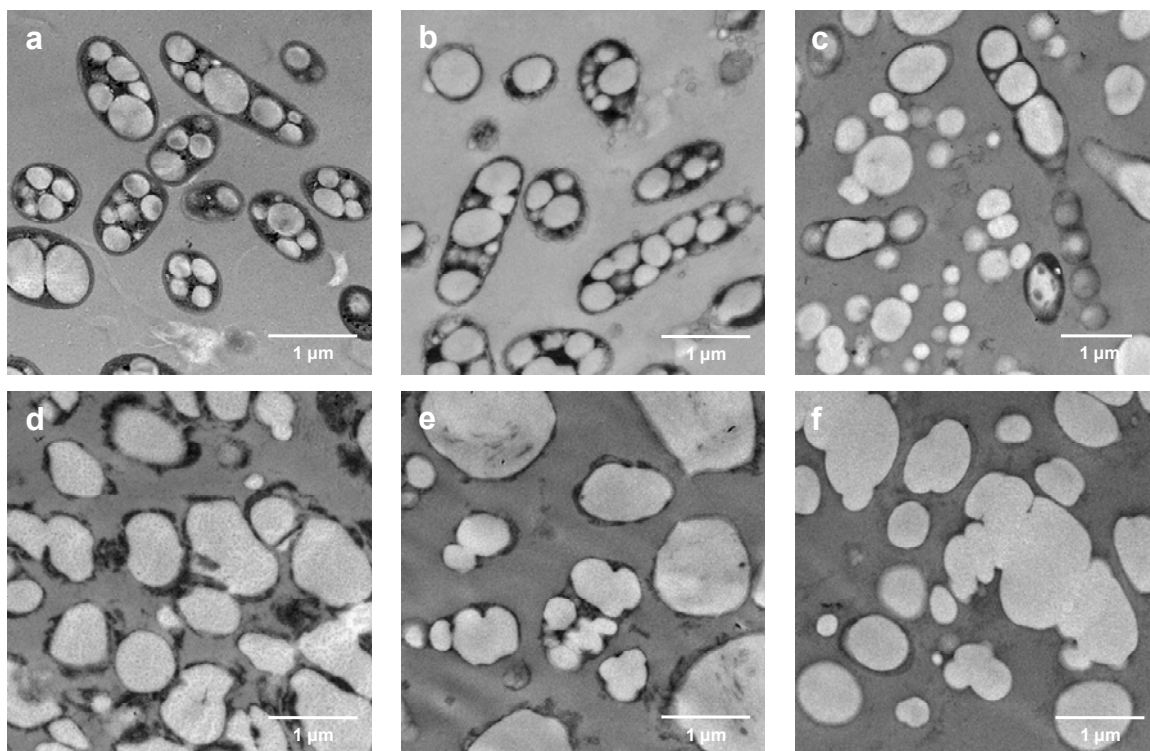


Figure 35. TEM images of PHB granules in varying environmental conditions arranged in order of increasing aggregation: (a) granules *in vivo* (pH 7); (b) native granules (pH 2); (c) alkaline granules (pH 12); (d) heated granules (120°C, 1 hr); (e) ultrasonicated granules (4.5 kJ/mL); (f) granules with surfactant (50 g/L SDS)

As seen in the figure, PHB granules *in vivo* are fully amorphous and exist as discrete, intracellular inclusion bodies (Figure 35a). When stored in the mild acidic solution (pH 2) the native granules showed very little crystallization (4-7%) and no aggregation because the granule membranes remained largely intact (Figure 35b). When 50 g/L SDS was added to the native granules (Figure 35f), there was extensive granule aggregation, suggesting that most of the granule membranes were ruptured or removed, and the surfactant may stabilize the granules in an amorphous state.

Mechanical force, such as centrifugation and ultrasonication, induced some crystallization in the native granules (~15%) and little to moderate aggregation. The degree of aggregation seems to be dependent on the state of the granule membrane – with little aggregation due to partially intact membranes from centrifugation (Figure 31b) and moderate aggregation due to ruptured membranes from ultrasonication (Figure 35e).

When dehydrated or subjected to harsh chemical conditions (i.e., acidic solution at high temperatures and alkaline solution at room temperature) the native granules became partially

crystalline (20-40%). Dehydration by freeze-drying removed intra-granule water, but did not otherwise change the native state of the granules. Therefore, the dehydrated granules crystallized significantly over 24 hours (32.71%) with no apparent granule aggregation (Figure 31a). In acidic solution (pH 2) at 120°C for 1 hr, the PHB was partial crystalline (22.52%) and showed moderate granule aggregation (Figure 35d). In alkaline solution (pH 12) at room temperature, the PHB was highly crystalline (40.59%) and seemed to exist as discrete granules of finite size (Figure 35c).

Comparing the environmental conditions that ruptured the granule membranes (i.e., surfactant, ultrasonication, acidic solution at high temperatures, and alkaline solution at room temperature), it is evident that granule aggregation decreases with increasing PHB crystallinity. It seems that the *in situ* crystallization of PHB toughens the granules, making them less susceptible to aggregation, whereas amorphous PHB molecules are free to entangle and aggregate.

6.2 Molecule Degradation

Further evidence that the crystallization of PHB toughens the granules is found by observing the molecular weight degradation of PHB granules with respect to the *in situ* crystallinity. Figure 36 shows the relative molecular weight (solid lines) and crystallinity (dashed lines) of the alkaline PHB granules (pH 12) at room temperature (red) and the heated PHB granules in acidic solution (pH 2) at 120°C (blue).

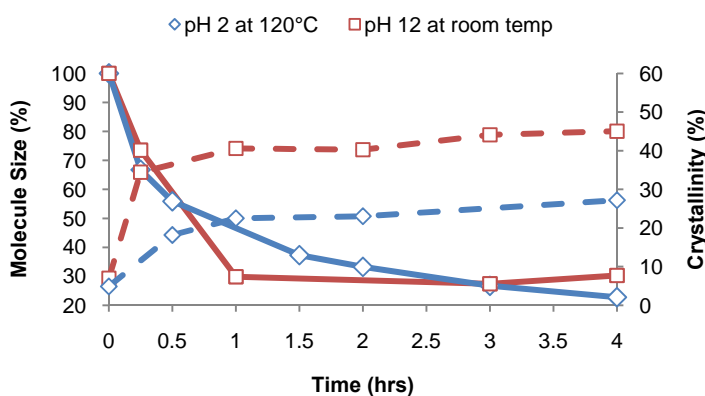


Figure 36. Molecular weight (solid lines) and *in situ* crystallinity (dashed lines) of heated granules (blue) and alkaline granules (red) over 4 hrs

As seen in the plot, the molecular weight of the heated granules continually declined with time, declining to a lesser degree, however, with increased crystallinity. The molecular weight of the alkaline granules, on the other hand, remained constant after 1 hr, which is attributed to the large increase in crystallinity (nearly twice that of the heated granules). The difference in molecule degradation is likely due to the extent of crystallization observed in the two cases. That is, the molecular weight did not continue to decline in harsh conditions as a result of the increase in crystallinity. Therefore, *in situ* crystallization toughens the granules against chemical attack. It seems that the more tightly-packed, ordered arrangements of the PHB molecules within the granules make the granules less susceptible to chemical degradation.

CHAPTER 7

PRACTICAL APPLICATIONS OF THE *IN SITU* CRYSTALLIZATION OF PHB

Understanding the *in situ* crystallization behavior of PHB granules in varying environmental conditions may lead to more efficient recovery methods to extract and purify PHA for commercial production, as well as, increase knowledge pertaining to the biological mechanisms associated with biopolymer production and degradation.

In PHA recovery, the goal is to separate PHA granules from the cells and remove any remaining impurities (i.e., non-PHA biomass) from the isolated granules. Current PHA recovery methods fall into one of two classes: selective and nonselective. Selective recovery is based on the concept of specificity, usually by solvent extraction or enzymatic digestion [50-52]. Selective recovery methods are appealing to researchers because they do not lead to PHA degradation [2, 50]. Even so, the technologies can be environmentally hazardous or expensive rendering them fairly uneconomical. Nonselective recovery refers to chemical digestion methods that utilize various nonselective chemical agents to attack and digest all non-PHA biomass of the hosting bacteria cells [25-28]. In contrast, chemical treatments are relatively safe and inexpensive. Still, one major drawback is that strong chemicals not only digest non-PHA biomass, but may also degrade PHA during treatment, reducing PHA yield, purity, and molecular weight [2, 28, 53].

In efforts to reduce the cost of PHA, recovery by chemical digestion has been investigated by many research groups [25, 26, 28, 39, 50, 53-56]. Even so, virtually none of these research groups have considered the *in situ* crystallization of PHA during recovery treatments. With the research provided here, it is possible to exploit the *in situ* crystallization behavior of PHA during various chemical treatments to toughen PHA granules against chemical attack, thereby limiting molecule degradation. Figure 37, for example, shows results from an experiment illustrating the “toughening” process. In this experiment, two solutions of PHB-containing cells were suspended in alkaline solution (pH 11) at room temperature over 3 hr. The first solution titled “acid+base” (blue) was subjected to an acid pretreatment (pH 2) at 100°C for 1 hr before the base treatment (pH 11) at room temperature. The second solution titled “base only” (red) was not subjected to an acid pretreatment. As seen in Figure 37, the “base only” cells (red) experienced a significant decrease in molecular weight of 60-70% and increase in PHB

content of about 10-15%. The partial crystallization induced by including the acid pretreatment in the “acid+base” cells (blue), however, toughened the PHB, reducing the molecular weight degradation to 20-40% and increasing the PHB purity to 15-25%.

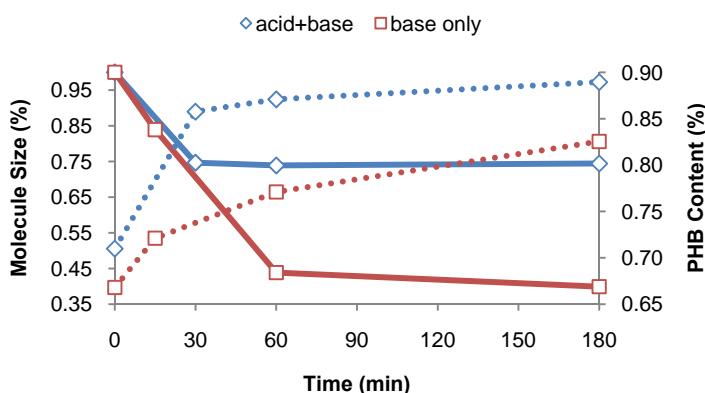


Figure 37. Molecular weight (solid lines) and PHB content (dotted lines) of PHB-containing cells treated at room temperature in alkaline solution (pH 11) with an acid pretreatment (pH 2) at 100°C for 1hr (blue) and without an acid pretreatment (red)

It may also be useful to exploit the amorphousness of PHA granules in different environments to promote granule aggregation. An example of this is the addition of surfactant (SDS) during chemical recovery treatments. Table 9 contains results from three parallel experiments (exact treatment processes not shown here) with increasing SDS concentration. As seen in the table, increasing concentrations of SDS from 0-20 g/L led to an increase in PHB content from 74-93% – nearly a 20% increase in purity with no additional molecule degradation. The significance of this result probably lies in the fact that SDS promotes granule aggregation; and, chemicals used during the treatment are only able to attack the outer surfaces of the granules. In other words, aggregation increases the average granule volume, and in turn, decreases the total surface area of granules susceptible to chemical attack.

Table 9. Addition of surfactant (SDS) during PHB recovery treatments

SDS (g/L)	PHB content	Molecular weight
0	74 %	46 %
10	85 %	54 %
20	93 %	51 %

Finally, the *in situ* crystallization of PHB may shed light on new methods to explore the biological mechanisms associated with the PHB granule. For instance, it is known that structural proteins, such as phasins, are partially responsible for stabilizing amorphous PHB granules *in vivo* [21-24]. However, the exact mechanism that these proteins use to “stabilize” the granules is unknown. Like the hydrogen bonded, pseudo-crosslinks that are formed by intra-granule water between amorphous PHB molecules [17, 23] (see Figure 4), it is of interest to determine the intra- and intermolecular interactions associated with the granule membrane. A better understanding of such biological mechanisms may also provide useful information on the *in vivo* synthesis and breakdown of PHB. Future researchers and biological engineers may find this information useful to develop more advanced biopolymers for eco-friendly and high-performance materials.

CHAPTER 8

FUTURE WORK

For future work related to the *in situ* crystallization of native PHB granules in varying environmental conditions, a variety of topics listed below may be worth exploring:

- a) Developing a more general model for the growth rate parameter dependent on both temperature and pH, such that $k = f(T, \text{pH})$;
- b) Developing an empirical model to describe the molecular weight of PHB in terms of *in situ* crystallinity, such that $M_v = f(X_i)$;
- c) Developing an empirical model to quantify and describe granule aggregation in terms of *in situ* crystallinity, such that $GA = f(X_i)$;
- d) Investigating granule crystallinity in simultaneous environmental conditions, such as adding SDS during ultrasonication of the PHB granules;
- e) Investigating granule crystallinity in sequential environmental conditions, such as heating then changing the pH of the PHB granules;
- f) Investigating alternate methods to induce *in situ* crystallization in PHB granules, such as seeding the granules with nano-particles to promote nucleation, similar to cloud seeding to promote precipitation;
- g) Investigating alternate methods to inhibit *in situ* crystallization in PHB granules, such as adsorption where surface adsorbates are added to the granules to promote aggregation and sedimentation;
- h) Determining the exact biological mechanisms that stabilize native PHB granules *in vivo* in an amorphous state;
- i) Developing more efficient PHA recovery methods to extract and purify PHA for the production of eco-friendly bioplastics.

REFERENCES

1. U.S. Product Supplied for Crude Oil and Petroleum Products.: Energy Information Administration, Department of Energy, 2008.
2. Luzier WD. Proceedings of the National Academy of Sciences of the United States of America 1992;89(3):839-842.
3. Anderson AJ and Dawes EA. Microbiological Reviews 1990;54:450-472.
4. Lee SY. Biotechnology and Bioengineering 1995;49:1-14.
5. Ojumu TV, Yu J, and Solomon BO. African Journal of Biotechnology 2004;3(1):18-24.
6. Barnard GN and Sanders JKM. Journal of Biological Chemistry 1989;264(6):3286-3291.
7. McChalicher CWJ and Srienc F. Journal of Biotechnology 2007;132(3):296-302.
8. Steinbuchel A and Valentin HE. FEMS Microbiology Letters 1995;128:219-228.
9. Byrom D. Polyhydroxyalkanoates. In: Mobley DP, editor. Plastic from microbes: microbial synthesis of polymers and polymer precursors. Munich: Hanser, 1994. pp. 5-33.
10. Allcock H, Lampe F, and Mark J. Contemporary Polymer Chemistry, 3rd ed. Upper Saddle River: Pearson Education, Inc, 2003.
11. Callister WDJ. Materials Science and Engineering: An Introduction, 6 ed. Hoboken: John Wiley & Sons, Inc., 2003.
12. Barham PJ, Keller A, Otun EL, and Holmes PA. Journal of Materials Science 1984;19:2781-2794.
13. Gunaratne LMWK, Shanks RA, and Amarasinghe G. Thermochimica Acta 2004;423:127-135.
14. Conti DS, Yoshida MI, Pezzin SH, and Coelho LAF. Thermochimica Acta 2006;450:61-66.
15. Cornibert J and Marchessault RH. Macromolecules 1975;8(3):296-305.
16. Padermshoke A, Katsumoto Y, Sato H, Ekgasit S, Noda I, and Ozaki Y. Spectrochimica Acta Part A 2005;61:541-550.
17. Sato H, Murakami R, Padermshoke A, Hirose F, Senda K, Noda I, and Ozaki Y. Macromolecules 2004;37(19):7203-7213.
18. Zhang J, Sato H, Noda I, and Ozaki Y. Macromolecules 2005;38:4274-4281.
19. Furukawa T, Sato H, Murakami R, Zhang J, Duan Y-X, Noda I, Ochiai S, and Ozaki Y. Macromolecules 2005;38:6445-6454.
20. Myerson AS. Molecular Modeling Applications in Crystallization. Cambridge University Press, 1999.
21. Grage K, Jahns AC, Parlane N, Palanisamy R, Rasiah IA, Atwood JA, and Rehm BHA. Biomacromolecules 2009;10:660-669.
22. Stuart ES, Tehrani A, Valentin HE, Dennis D, Lenz RW, and Fuller RC. Journal of Biotechnology 1998;64:137-144.
23. Sudesh K, Abe H, and Doi Y. Progress in Polymer Science 2000;25:1503-1555.
24. Jendrossek D. Applied Microbiology and Biotechnology 2007;74:1186-1196.
25. Chen Y, Chen J, Yu C, Du G, and Lun S. Process Biochemistry 1999;34:153-157.
26. Choi J-i and Lee SY. Biotechnology and Bioengineering 1999;62(5):546-553.

27. Herron JS, King JD, and White DC. *Applied and Environmental Microbiology* 1978;35(2):251-257.
28. Hahn SK, Chang YK, and Lee SY. *Applied and Environmental Microbiology* 1995;61:34-39.
29. Horowitz DM and Sanders JKM. *Journal of the American Chemical Society* 1994;116(7):2695-2702.
30. Smith B. *Infrared Spectral Interpretation: A Systematic Approach*. Boca Raton: CRC Press, 1999.
31. Gunzler H and Gremlich H-U. *IR Spectroscopy: An Introduction*. Weinheim: Wiley-VCH 2002.
32. Ward MD. *Chemical Reviews* 2001;101(6):1697-1726.
33. Xu J, Guo B-H, Yang R, Wu Q, Chen G-Q, and Zhang Z-M. *Polymer* 2002;43:6893-6899.
34. Li J, Zhou C, Wang G, Tao Y, Liu Q, and Li Y. *Polymer Testing* 2002;21(5):583-589.
35. Anderson KL and Goldbeck-Wood G. *Polymer* 2000;41(25):8849-8855.
36. Liu M, Zhao Q, Wang Y, Zhang C, Mo Z, and Cao S. *Polymer* 2003;44(8):2537-2545.
37. Cheng SZD and Lotz B. *Polymer* 2005;46(20):8662-8681.
38. Bradford MM. *Analytical Biochemistry* 1976;72:248.
39. Hesselmann RPX, Fleischmann T, Hany R, and Zehnder AJB. *Journal of Microbiological Methods* 1999;35:111-119.
40. Marchessault RH, Okamura K, and Su CJ. *Macromolecules* 1970;3:735-740.
41. Bloembergen S, Holden DA, Hamer GK, Bluhm TL, and Marchessault RH. *Macromolecules* 1986;19:2865-2871.
42. Chen C, Yu PH, and Cheung MK. *Journal of Applied Polymer Science* 2005;98:736-745.
43. Hu Y, Zhang J, Sato H, Futami Y, Noda I, and Ozaki Y. *Macromolecules* 2006;39(11):3841-3847.
44. Cheng M-L, Sun Y-M, Chen H, and Jean YC. *Polymer* 2009;50:1957-1964.
45. Wu Q, Tian G, Sun S, Noda I, and Chen G-Q. *Journal of Applied Polymer Science* 2001;82(4):934-940.
46. Tang B and Wu P. *Vibrational Spectroscopy* 2008;1665:1-7.
47. Chen C, Fei B, Peng S, Zhuang Y, Dong L, and Feng Z. *European Polymer Journal* 2002;38(8):1663-1670.
48. Ziaee Z and Supaphol P. *Polymer Testing* 2006;25(6):807-818.
49. An Y, Dong L, Li L, Mo Z, and Feng Z. *European Polymer Journal* 1999;35(3):365-369.
50. Jacquelin N, Lo C-W, Wei Y-H, Wu H-S, and Wang SS. *Biochemical Engineering Journals* 2008;39:15-27.
51. Yasotha K, Aroua M, Ramachandran K, and Tan I. *Biochemical Engineering Journals* 2006;30:260-268.
52. Lee SY. *Biotechnology and Bioengineering* 1996;49:1-14.
53. Yu J, Plackett D, and Chen LXL. *Polymer Degradation and Stability* 2005;89:289-299.
54. Chen GQ, Zhang G, Park SJ, and Lee SY. *Applied Microbiology and Biotechnology* 2001;57:50-55.
55. Hee Pv, Elumbaring ACMR, Lans RGJMvd, and Wielen LAMvd. *Journal of Colloid and Interface Science* 2006;297:595-606.
56. Yu J and Stahl H. *Bioresource Technology* 2008;99:8042-8048.